Accepted Manuscript

Triazolopyridinyl-acrylonitrile derivatives as antimicrotubule agents: Synthesis, *in vitro* and *in silico* characterization of antiproliferative activity, inhibition of tubulin polymerization and binding thermodynamics

Irene Briguglio, Erik Laurini, Maria Antonietta Pirisi, Sandra Piras, Paola Corona, Maurizio Fermeglia, Sabrina Pricl, Antonio Carta

PII: S0223-5234(17)30780-8

DOI: 10.1016/j.ejmech.2017.09.065

Reference: EJMECH 9780

To appear in: *European Journal of Medicinal Chemistry*

Received Date: 12 July 2017

Revised Date: 27 September 2017

Accepted Date: 28 September 2017

Please cite this article as: I. Briguglio, E. Laurini, M.A. Pirisi, S. Piras, P. Corona, M. Fermeglia, S. Pricl, A. Carta, Triazolopyridinyl-acrylonitrile derivatives as antimicrotubule agents: Synthesis, *in vitro* and *in silico* characterization of antiproliferative activity, inhibition of tubulin polymerization and binding thermodynamics, *European Journal of Medicinal Chemistry* (2017), doi: 10.1016/j.ejmech.2017.09.065.

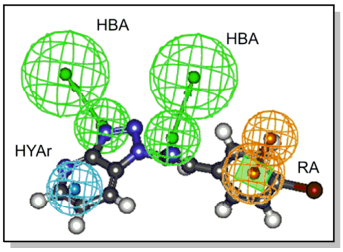

3D pharmacophore model

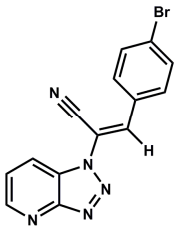

Compound 6c

$EC_{50(Hela)}$ = 0.65 ± 0.14 μM

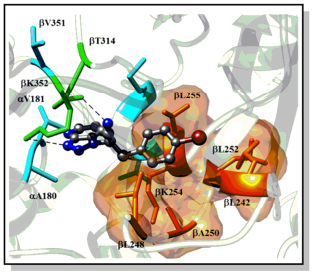

Tubulin/6c complex

Triazolopyridinyl-acrylonitrile derivatives as antimicrotubule agents: synthesis, *in vitro* and *in silico* characterization of antiproliferative activity, inhibition of tubulin polymerization and binding thermodynamics

Irene Briguglio[a,1], Erik Laurini[b,c,1], Maria Antonietta Pirisi[a], Sandra Piras[a], Paola Corona[a], Maurizio Fermeglia[b,c], Sabrina Pricl[b,c,*], Antonio Carta[a,*]

[a] Dipartimento di Chimica e Farmacia, Università degli Studi di Sassari, via Muroni 23A, 07100 Sassari, SS, Italy

[b] Molecular Simulation Engineering (MOSE) Laboratory, DEA, University of Trieste, Piazzale Europa 1, 34127 Trieste, Italy

[c] National Interuniversity Consortium for Material Science and Technology (INSTM), Research Unit MOSE-DEA, University of Trieste, 34127 Trieste, Italy

[*] Corresponding authors. acarta@uniss.it (A. Carta), sabrina.pricl@dia.units.it (S. Pricl).

[1] These authors equally contributed to this work.

Abstract

In this paper we report the synthesis, *in vitro* anticancer activity, and the experimental/computational characterization of mechanism of action of a new series of *E* isomers of triazolo[4,5-*b*/*c*]pyridin-acrylonitrile derivatives (**6c-g**, **7d-e**, **8d-e**, **9c-f**, **10d-e**, **11d-e**). All new compounds are endowed with moderate to interesting antiproliferative activity against 9 different cancer cell lines derived from solid and hematological human tumors. Fluorescence-based assays prove that these molecules interfere with tubulin polymerization. Furthermore, isothermal titration calorimetry (ITC) provides full tubulin/compound binding thermodynamics, thereby ultimately qualifying and quantifying the interactions of these molecular series with the target protein. Lastly, the analysis based on the tight coupling of *in vitro* and *in silico* modelling of the interactions between tubulin and the title compounds allows to propose a molecular rationale for their biological activity.

Keywords: Triazolo[4,5-*b*/*c*]pyridin-acrylonitriles, Antiproliferative activity, Tubulin polymerization, Molecular modeling, Isothermal titration calorimetry, Fluorescence-based assays

1. Introduction

Incontrollable cell proliferation constitute the basis for malignant tumor emergence. Various chemotherapeutic agents can reach different molecular targets affecting the proliferation process.

Among these, structurally complex natural products such as paclitaxel, vinblastine, and vincristine are potent microtubules-targeting drugs [1] widely used in the treatment of cancer. Microtubules are cytoskeletal polymers that play a key role in the regulation of processes such as segregation of chromosomes during mitosis, intracellular transport and cellular shape. Their basic structural unit is constituted by assembled/disassembled α,β-tubulin heterodimers in a dynamic system. Specific binding sites for inhibitors can be identified on the heterodimers [2]. Consequent to this interaction, inhibitors suppress tubulin dynamic instability and interfere with microtubule functions, including mitotic spindle formation. This event blocks mitosis and arrests the cell cycle in the G2/M phase, ultimately leading to apoptosis [3].

Microtubule-targeting agents are classified into two categories: 1) molecules binding to the vinblastine and colchicine binding site and inhibiting tubulin assembly are defined as microtubule destabilizing agents; 2) molecules binding to the tubulin paclitaxel-binding site are defined as microtubule-stabilizing agents [4]. Actually, colchicine and its structurally analogues are not used in clinical settings as they are too toxic at therapeutic doses. However, synthetic compounds able to bind to the colchicine-binding site are currently undergoing clinical development and evaluation in patients with a wide array of cancers [5].

Recently we reported the synthesis and evaluation as antiproliferative agents of some benzotriazol-(1)-yl-3-phenylacrylonitrile derivatives [6, 7], and demonstrated that this series of compounds act on the G2/M phase of the cell cycle. This behavior was consistent with a possible tubulin binding activity; accordingly, we confirmed this hypothesis using competition experiments in which the reference compound (*E*-2-(1*H*-benzo[*d*][1,2,3]triazol-1-yl)-3-(benzo[*d*][1,3]dioxol-5-yl)acrylonitrile strongly displaced radio labeled colchicine from its tubulin binding site, with an IC_{50} value lower than colchicine itself (0.85 μM and 1.02 μM, respectively) [8].

Molecular modeling studies of the putative binding mode of this series of compounds on tubulin further supported this finding [8]. As previously observed, substitutions with electron donor (i.e methyl group) and electro withdrawing (i.e. chlorine) groups on the phenyl moiety of benzotriazole did not lead to enhanced activity, unsubstituted benzotriazole remaining the most promising scaffold. Actually, with the twofold goal of improving the antiproliferative potency and the physicochemical properties of these derivatives, we modified the main scaffold and substituted the benzotriazole group with a 3*H*-[1,2,3]triazolo[4,5-*b*]pyridine or a 3*H*-[1,2,3]triazolo[4,5-*c*]pyridine moiety.

Indeed, we speculated that the steric hindrance exerted by the presence of a bulky group (e.g., methyl or chlorine) on the benzotriazole moiety could be more deleterious to the biological activity of the resulting compounds than their electronic contribution. So we decided to preserve an

electron-withdrawing group on this moiety, maintaining at the same time the steric hindrance only on the other phenyl, to speed up the *Knoevenagel condensation* and to obtain *E*-stereoselective synthesis, as previously observed [6-9]. For these reasons, we chose to introduce a nitrogen on the phenyl side of benzotriazole moiety, simultaneously evaluating the relevance of its relative position. The electron-withdrawing nitrogen in pyridine makes the deprotonated intermediate of the *Knoevenagel condensation* more stable, affording exclusively the thermodynamically more stable *E*-derivatives. Spectral and analytical data obtained for all new compounds are in accordance with those of the previously described counterparts [6-9], and support the assigned chemical structure.

We finally synthesized a series of triazolo[4,5-*b*/*c*]pyridin-acrylonitrile derivatives, maintaining the same feature in the heterocyclic moiety, while the phenyl-moiety of the side chain was functionalized using a variety of groups chosen from those endowed with the most antiproliferative activity in the previous series (Br, CH_3, OCH_3, 3,4,5(OCH_3)$_3$), or totally substituted with a naphtyl moiety, as depicted in Figure 1.

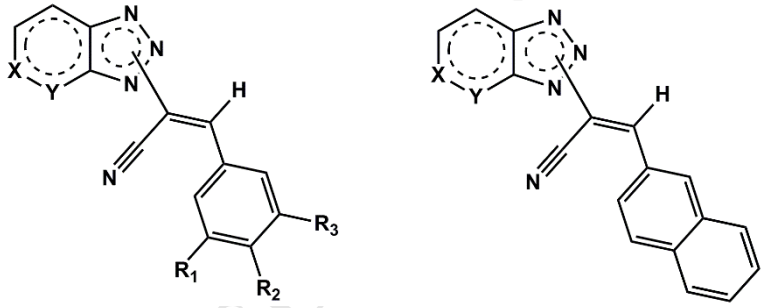

Figure 1. General chemical structures for the triazolo[4,5-*b*/*c*]pyridin-acrylonitrile derivatives synthesized in this work.

All new derivatives were synthesized following a consolidated chemistry [9]. From each triazolopyridine intermediate (**1a,b** of Scheme 1), we obtained 3 series of *E* isomers from substitution on each of the N atoms (N1-3) of the triazole moiety (**2-4a,b** of Scheme 1). All compounds were evaluated for antiproliferative activity against a panel of cell lines derived from hematological and solid human tumors. To investigate whether the antiproliferative activities of the synthesized compounds were related to an interaction with tubulin, *in vitro* inhibition of tubulin polymerization was determined using a fluorescence-based assay. The preliminary determination of the dissociation constant K_d of the new compounds from tubulin was carried out *in vitro* by fluorescence spectroscopy. The values of K_d and the tubulin binding site were then confirmed for all compounds by isothermal titration calorimetry (ITC). Finally, a molecular modelling study was carried out to draw a molecular rationale for the binding of these new series of molecules to tubulin.

2. Chemistry

The intermediate compound 3*H*-[1,2,3]triazolo[4,5-*b*]pyridine (**1a**) was commercially available while the 3*H*-[1,2,3]triazolo[4,5-*c*]pyridine (**1b**) was prepared in good yield via diazotation reaction with $NaNO_2$ starting from the pyridine-3,4-diamine. The 3*H*-[1,2,3]triazolo[4,5-*b*/*c*]pyridine-1,2,3-carbonitrile derivatives (**2-4a,b**) were in turn prepared by nucleophilic substitution reaction of triazolo derivatives (**1a,b**) with chloroacetonitrile in dimethylformamide (DMF) in the presence of triethylamine (Et_3N) (Scheme 1), following a procedure reported in details in our previous work [9]. In particular the yields of the condensation of **1a** and **1b** with chloroacetonitrile afforded the mixture of compounds **2-4a**, in 78 % in the ratio **2a** (24%), **3a** (16%), **4a** (38%); and compounds **2-4b**, in 63 % in the ratio **2b** (19%), **3b** (16%), **4b** (28%).

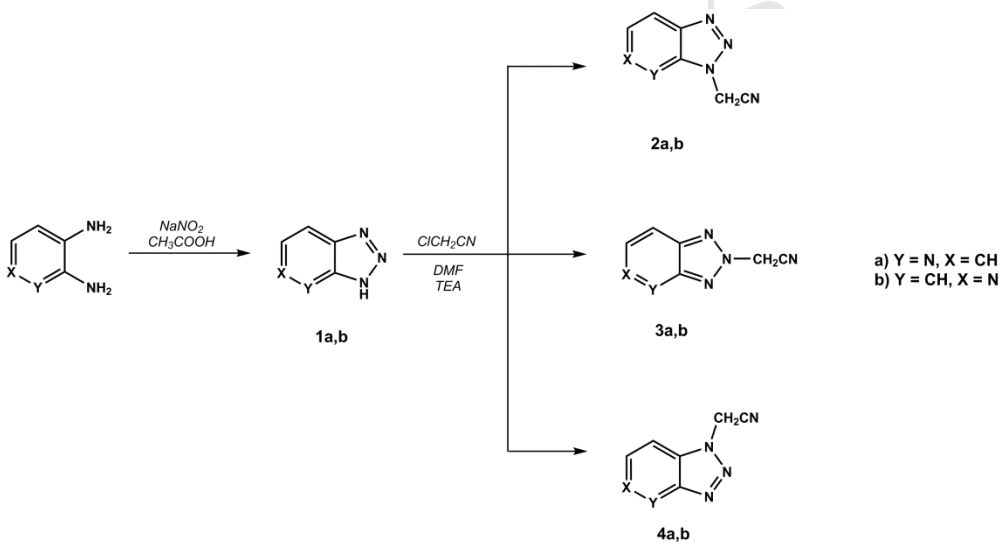

Scheme 1: Synthesis of intermediate 3*H*-[1,2,3]triazolo[4,5-*b*/*c*]pyridine-1,2,3-carbonitrile (**2-4a,b**).

Finally, the synthesis of triazolo[4,5-*b*/*c*]pyridin-acrylonitrile derivatives (**6c-g**, **7d-e**, **8d-e**, **9c-f**, **10d-e**, **11d-e**) was accomplished by Knoevenagel condensation of intermediates (**2-4a,b**) with the appropriate commercially available aldehydes (**5c-g**), in toluene at reflux in the presence of Et_3N (Scheme 2) [6]. In this new series, between the two possible geometric isomers (*E*/Z), *E*-isomers were obtained as the sole product. Spectral and analytical data obtained for all new compounds were in accordance with those of previously described derivatives [6, 11, 12] and supported the assigned chemical structure.

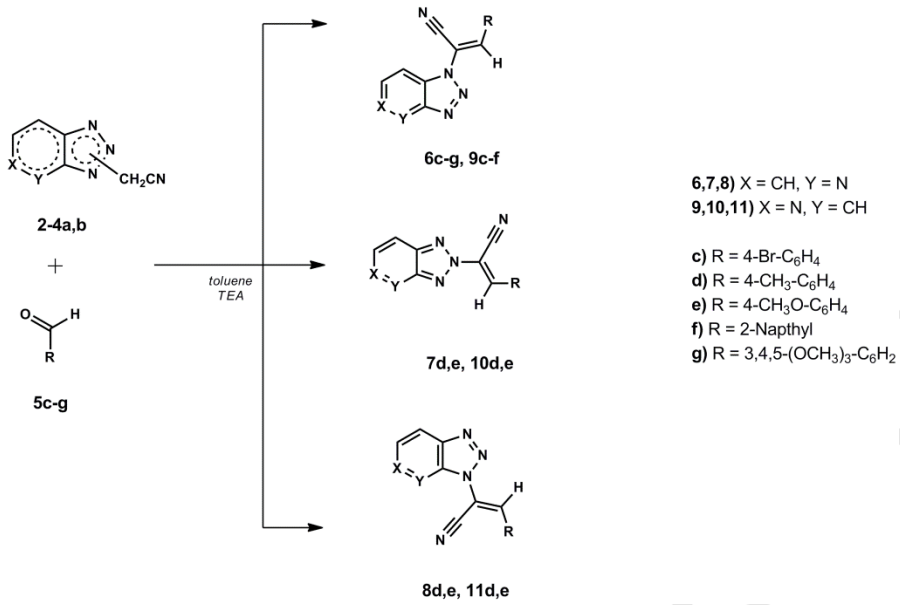

Scheme 2: Synthesis of triazolo[4,5-*b*/*c*]pyridin-acrylonitrile derivatives **6c-g**, **7d-e**, **8d-e**, **9c-f**, **10d-e** and **11d-e**.

3. *In vitro* cell growth inhibition assay

To characterize the tumor cell growth inhibitory profile of all new synthesized compounds **6c-g**, **7d-e**, **8d-e**, **9c-f**, **10d-e** and **11d-e**, their antiproliferative activity against a panel of 9 cell lines derived from different human tumors was evaluated (Table 1). From these data, a structure-activity relationship could be established based on the variation of the position of the pyridine N atom, and of the nature and position of the substituent R on the molecular scaffold (Scheme 1). As can be seen by comparing corresponding data for (**6-8**) and (**9-11**) molecular series, the position of the pyridine N atom only marginally affects the activity of the relevant compounds, those belonging to the **6-8** series being slightly more active than the corresponding **9-11** derivatives (e.g., compare EC_{50}(**6e**) = 10.3 - 36.8 μM and EC_{50} (**9e**) = 13.3 – 41.4 μM, Table 1). On the contrary, for both compound series (**6-8**) and (**9-11**) the presence of the R substituent either at position 1 or 3 of the triazole ring provides better antiproliferative activity with respect to those carrying R at position 2 in all cell lines. Thus, taking the HeLa cell line as a proof-of-concept, the range of EC_{50} values for compound **6d** (0.97 μM, Table 1), featuring the substituent R = 4-CH_3-C_6H_4 at position 1, are significantly lower than those of the corresponding isomer **7d** (25.1 μM, Table 1), in which the same R locates at position 2 of the triazole ring. Also, the derivatives featuring bulkier Rs at positions 1 of triazolo[4,5-*b*]pyridine and]triazolo[4,5-*c*]pyridin derivatives, i.e., 2-naphtyl (**6f**, EC_{50} = 17.2 μM and **9f**, EC_{50} = 22.2 μM) and 3,4,5-(CH_3O)-C_6H_2 (**6g**, EC_{50} = 13.8 μM) show significantly lower potency with respect to all other compounds bearing less sterically hindered groups at the same sites (Table 1).

Table 1. Half-maximal inhibitory concentration (EC_{50}, μM) of compounds (**6-8**) and (**9-11**) in different human cancer cell lines. EC_{50} values are the means of three independent determinations.

Cpd	Pos. "N"	R	[a]HeLa	[b]DU145	[c]CCRF-CEM	[d]MCF-7	[e]A-427	[f]LCLC 103H	[g]DAN-G	[h]5637	[i]HL-60
6c	1	4-Br-C_6H_4	**0.65 ± 0.14**	**0.98 ± 0.31**	**0.76 ± 0.15**	7.1 ± 0.7	1.2 ± 0.6	2.1 ± 0.4	15.4 ± 2.2	1.9 ± 0.6	12.2 ± 1.9
6d	1	4-CH_3-C_6H_4	**0.97 ± 0.23**	1.4 ± 0.6	**0.99 ± 0.18**	10.9 ± 2.1	1.6 ± 0.6	1.9 ± 0.2	18.9 ± 2.1	2.2 ± 0.5	10.9 ± 1.3
6e	1	4-CH_3O-C_6H_4	10.3 ± 1.2	12.7 ± 2.2	7.4 ± 0.6	25.6 ± 1.3	8.9 ± 0.4	10.2 ± 1.0	36.8 ± 2.3	12.6 ± 1.8	27.9 ± 2.0
6f	1	2-Naphtyl	17.2 ± 1.9	39.2 ± 1.7	15.6 ± 2.2	59.8 ± 2.6	17.4 ± 1.1	17.1 ± 1.3	78.3 ± 3.4	19.4 ± 1.2	68.3 ± 2.8
6g	1	3,4,5-$(CH_3O)_3$-C_6H_2	13.8 ± 1.4	15.8 ± 1.5	11.3 ± 1.6	29.1 ± 1.8	11.6 ± 1.0	13.8 ± 1.1	40.1 ± 2.8	12.5 ± 1.1	37.1 ± 1.6
7d	2	4-CH_3-C_6H_4	25.1 ± 2.3	22.4 ± 1.9	32.6 ± 2.3	48.5 ± 2.0	39.6 ± 1.6	37.5 ± 1.9	88.1 ± 4.2	33.1 ± 1.7	78.3 ± 3.1
7e	2	4-CH_3O-C_6H_4	38.6 ± 2.5	31.6 ± 1.8	33.7 ± 1.7	67.8 ± 2.4	45.8 ± 1.3	51.4 ± 2.2	90.6 ± 3.9	49.2 ± 2.3	69.5 ± 2.9
8d	3	4-CH_3-C_6H_4	3.3 ± 0.8	2.7 ± 1.1	1.8 ± 0.5	15.4 ± 1.9	3.9 ± 0.2	2.2 ± 0.3	26.7 ± 1.5	4.8 ± 0.3	31.1 ± 2.2
8e	3	4-CH_3O-C_6H_4	11.1 ± 1.3	12.6 ± 1.4	8.5 ± 0.9	31.0 ± 2.3	10.7 ± 1.8	12.6 ± 1.5	49.8 ± 2.0	15.3 ± 1.2	49.9 ± 2.4
Cpd	Pos. "N"	R	[a]HeLa	[b]DU145	[c]CCRF-CEM	[d]MCF-7	[e]A-427	[f]LCLC 103H	[g]DAN-G	[h]5637	[i]HL-60
9c	1	4-Br-C_6H_4	1.6 ± 0.8	1.2 ± 0.3	1.2 ± 0.3	8.5 ± 0.4	2.8 ± 0.8	3.2 ± 0.7	20.0 ± 2.6	2.9 ± 0.2	17.5 ± 2.2
9d	1	4-CH_3-C_6H_4	2.3 ± 0.3	2.8 ± 0.4	2.5 ± 0.2	14.4 ± 1.9	3.5 ± 0.6	4.1 ± 0.4	19.2 ± 2.2	3.3 ± 0.4	18.6 ± 2.0
9e	1	4-CH_3O-C_6H_4	13.1 ± 1.6	13.8 ± 1.9	9.9 ± 0.7	29.5 ± 1.8	10.1 ± 1.0	12.9 ± 1.1	41.4 ± 2.5	17.1 ± 1.5	32.9 ± 2.1
9f	1	2-Naphtyl	22.2 ± 1.4	36.7 ± 1.5	22.1 ± 1.8	68.6 ± 2.2	24.4 ± 1.3	27.1 ± 1.7	81.5 ± 2.9	23.6 ± 1.7	70.5 ± 2.2
10d	2	4-CH_3-C_6H_4	32.0 ± 2.6	33.7 ± 1.8	30.2 ± 2.1	44.8 ± 2.9	41.2 ± 2.1	41.5 ± 1.8	90.9 ± 3.9	35.2 ± 1.1	85.1 ± 3.6
10e	2	4-CH_3O-C_6H_4	44.1 ± 2.7	41.1 ± 2.2	43.6 ± 2.0	77.3 ± 2.7	52.1 ± 2.8	57.7 ± 3.0	98.8 ± 3.1	50.6 ± 2.1	72.8 ± 3.1
11d	3	4-CH_3-C_6H_4	9.5 ± 1.1	8.2 ± 1.6	7.8 ± 0.3	28.2 ± 2.1	9.9 ± 1.1	7.5 ± 0.9	41.4 ± 1.8	10.6 ± 1.2	39.3 ± 2.5
11e	3	4-CH_3O-C_6H_4	17.6 ± 1.7	15.8 ± 1.2	16.3 ± 1.1	38.6 ± 3.0	17.7 ± 2.2	16.9 ± 1.8	57.2 ± 2.6	20.1 ± 2.1	59.3 ± 2.8
Colchicine[j]		-	0.027 ± 0.003	0.018 ± 0.002	0.021 ± 0.003	0.061 ± 0.005	0.045 ± 0.001	0.070 ± 0.005	0.059 ± 0.006	0.053 ± 0.009	0.0086 ± 0.008

[a]HeLa = ACC-57 (cervix carcinoma); [b]DU145 = ACC-261 (prostate carcinoma); [c]CCRF-CEM = ACC-240 (T-cell leukemia); [d]MCF-7 = ACC-115 (breast adenocarcinoma); [e]A-427 = ACC-234 (small cell lung carcinoma); [f]LCLC 103H = ACC-384 (large cell lung carcinoma); [g]DAN-G = ACC-249 (pancreas carcinoma); [h]5637 = ACC-35 (urinary bladder carcinoma); [i]HL-60 = ACC-3 (acute myeloid leukemia); [j]Colchicine = reference compound.

Within the entire pool of synthesized molecules, compound **6c** in which R = 4-Br-C_6H_4 was found to be the most potent antiproliferative agent, with EC_{50} values in the range 0.65-15.4 μM towards

all cell lines. In detail, compound **6c** inhibited the growth of HeLa cells with a half-maximal inhibitory concentration EC_{50} = 0.65 ± 0.14 μM (Figure 2A). Similarly, inhibition of DU145 and CCRF-CEM cell growth was achieved by the same compound with EC_{50} of 0.98 ± 0.31 and 0.76 ± 0.15 μM, respectively. Good antiproliferative activity for **6c** was also observed against breast (MCF-7), small (A-427)/non small (LCLC 103H) cell lung, and urinary bladder (5637) carcinoma cell lines (Table 1), whilst moderate activity (10 -20 μM) was recorded in the case of acute myeloid leukemia (HL-60) and pancreatic carcinoma cell lines (DAN-G, Figure 2B).

Figure 2. Compound **6c** inhibition of proliferation of HeLa (A) and DAN-G (B) cells.

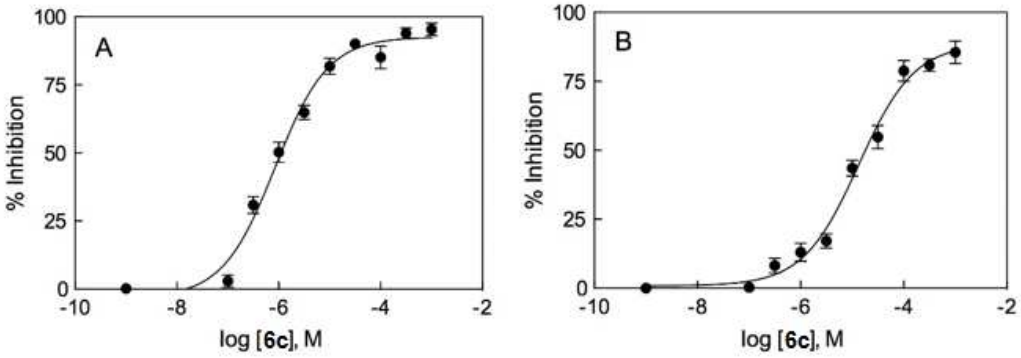

Nonspecific cytotoxicity of anticancer drugs may constitute a major obstacle in cancer chemotherapy. Accordingly, we also preliminarily determined the effect of the two most promising compounds, **6c** and **6d**, on the proliferation activity of three normal cell lines (i.e., human peripheral mononuclear blood cells (HPMBC), human pulmonary fibroblasts (HPF), and human prostate epithelial cells (HPEC), Table S1). Comparison of the relevant EC_{50} values with those of the pertinent malignant cell lines (Table 1) reveals that both compounds are endowed - on average – with substantial less normal cell cytotoxicity (28.5-35 x for HPEC, 14-17 x for HPF, and 40-55 x for HPEC, respectively).

4. In vitro tubulin polymerization assay

To investigate whether the antiproliferative activities of compounds (**6-8**) and (**9-11**) were related to an interaction with tubulin, they were assayed for their inhibitory effects on tubulin polymerization (ITP) *in vitro* using a fluorescence-based tubulin polymerization assay. As shown in Figure 3, the hit compound **6c** was able to inhibit the rate and extent of tubulin assembly in a concentration-dependent manner, the half-maximal inhibition (ITP IC_{50}) occurring at 17.2 ± 0.9 μM.

Figure 3. (A) *In vitro* concentration-dependent inhibition of tubulin polymerization by compound **6c** (ITP IC_{50} = 17.2 ± 0.9 μM). Symbol legend: ●, 0 μM; ■, 5 μM; ▲, 10 μM; ◆, 15 μM; ○, 20 μM; □, 30 μM; △, 40 μM. (B)

Determination of **6c** ITP IC_{50} value by sigmoidal fitting of steady state levels of tubulin assembly from panel A vs. drug concentration. Three independent sets of experiments were performed; however, only one of the sets is shown for clarity.

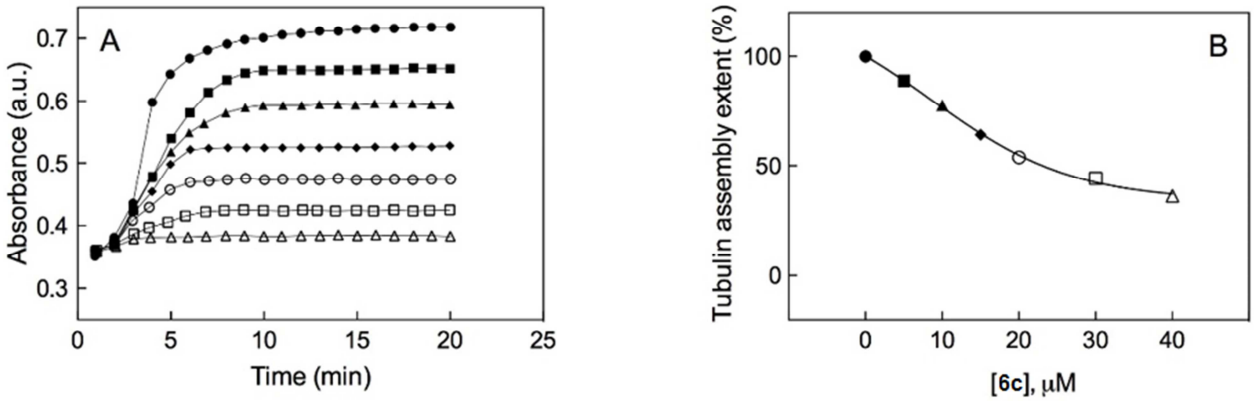

Compounds **6d** was also found to inhibit tubulin assembly with an ITP IC_{50} of 23.9 ± 1.2 μM. In the (**9-11**) series, only compound **9c** was endowed with appreciable tubulin depolymerization activity, with ITP IC_{50} = 29.1 ± 1.5 μM. Under similar conditions, four reference compounds - colchicine, nocodazole, podophyllotoxin, and vinblastine sulfate - exhibited significantly more potent microtubule depolymerization activity, with ITP IC_{50} of 1.32 ± 0.23, 0.81 ± 0.07, 0.26 ± 0.09, and 0.15 ± 0.07 μM, respectively. Accordingly, compounds **6c**, **6d**, and **9c** can be classified as moderate tubulin polymerization inhibitors. Of note, we observe that the determined concentrations required to inhibit tubulin polymerization by these three compounds are much higher than those required for cytotoxicity, a phenomenon however well documented in the literature [see, for instance, 13-16].

All other compounds had ITP IC_{50} values > 30 μM; as such, they were regarded to have only weak activity as inhibitors of tubulin polymerization.

Tubulin polymerization inhibitors usually interfere with the G2/M phase of the cell cycle by altering the dynamics of tubulin polymerization, ultimately triggering cell death via apoptotic pathways. Therefore, we considered interesting to study the effect exerted by the two lead compounds, **6c** and **6d**, on cell cycle progression by flow cytometry experiments (Figure S2). The results show that untreated (control) prostate carcinoma cells DU145, taken as a proof-of-concept, distributed in the Sub-G1 (8.7%), G0/G1 (78%), S (3.6%), and G2/M (9.5%) phase. On the other hand, both compounds arrested most of the cells in the G2/M phase (71.1% and 69.3% for **6c** and **6d**, respectively, Figure S2). Collectively, these results are consistent with the indication that these molecules can act as efficient mitotic blockers.

5. Preliminary determination of the dissociation constant of compounds 6c to tubulin in vitro by fluorescence spectroscopy

According to the results presented above, **6c** was able to prevent the assembly of tubulin with ITP EC_{50} < 20 μM. Therefore, we performed a preliminary investigation to determine whether **6c** directly interacted with tubulin. Compound **6c** quenched the tryptophan fluorescence of tubulin in a concentration-dependent fashion, thereby confirming the interaction between the small molecule and the protein (Figure 4A).

Figure 4. (A) Quenching of intrinsic tryptophan fluorescence of tubulin by different concnetrations of compound **6c**. Symbol legend: ●, 0 μM; ■, 5 μM; ▲, 10 μM; ◆, 15 μM; ○, 20 μM; □, 30 μM; △, 40 μM. Tubulin concentration = 2 μM. (B) Differential change in fluorescence intensity of tubulin upon binding of compound **6c**. Three independent sets of experiments were performed; however, only one of the sets is shown for clarity.

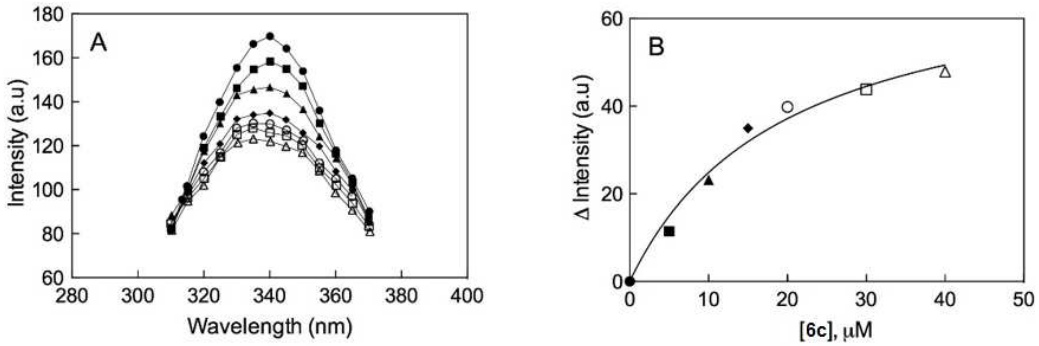

The dissociation constant (K_d) of compound **6c** from tubulin - obtained by fitting the maximum tubulin fluorescence intensity change as a function of compound concentration (Figure 4B) - was found to be equal to 19.6 ± 1.0 μM. Based on this preliminary information and with the twofold purpose of obtaining 1) accurate K_d values for all compounds and 2) a full thermodynamic characterization of compound/tubulin interactions (indispensible for validation of the modeling results, *vide infra*), further binding studies were conducted by ITC.

6. Determination of the dissociation constant and tubulin binding site of compounds (6-8) and (9-11) by Isothermal Titration Calorimetry (ITC)

In order to investigate the tubulin binding affinities of all (**6-8**) and (**9-11**) compounds in detail, thermodynamic studies were conducted using isothermal titration calorimetry (ITC). The averaged dissociation constant (K_d), binding free energy (ΔG_b), enthalpy (ΔH_b) and entropy terms ($-T\Delta S_b$) resulting from three independent ITC measurements on each compound are listed in Table 2, while Figure 5 displays some representative ITC results and fitting curves for compounds belonging to both (**6-8**) and (**9-11**) series.

Table 2. ITC determined thermodynamic data of compounds (**6-8**) and (**9-11**) binding to tubulin. $\Delta G_b = \Delta H_b - T\Delta S_b$. $\Delta G_b = RT \ln K_d$. n = number of binding site. All experiments were run in triplicate. Errors on ΔH_b are within 5%.

Cpd	Pos. "N"	R	K_d (μM)	ΔG_b (kcal/mol)	ΔH_b (kcal/mol)	$T\Delta S_b$ (kcal/mol)	n (-)
6c	1	4-Br-C_6H_4	16.4	-6.75	-9.21	2.46	0.98
6d	1	4-CH_3-C_6H_4	22.0	-6.57	-8.96	2.39	1.00
6e	1	4-CH_3O-C_6H_4	192	-5.24	-7.35	2.11	0.95
6f	1	2-Naphtyl	385	-4.82	-6.87	2.05	0.97
6g	1	3,4,5-$(CH_3O)_3$-C_6H_2	241	-5.10	-7.16	2.06	1.01
7d	2	4-CH_3-C_6H_4	581	-4.56	-6.81	2.25	0.96
7e	2	4-CH_3O-C_6H_4	763	-4.40	-6.75	2.35	1.02
8d	3	4-CH_3-C_6H_4	58.4	-5.97	-7.84	1.87	0.98
8e	3	4-CH_3O-C_6H_4	217	-5.17	-7.23	2.06	0.99
Cpd	Pos. "N"	R	K_d (μM)	ΔG_b (kcal/mol)	ΔH_b (kcal/mol)	$T\Delta S_b$ (kcal/mol)	n (-)
9c	1	4-Br-C_6H_4	33.9	-6.30	-8.63	2.33	1.00
9d	1	4-CH_3-C_6H_4	64.5	-5.91	-7.79	1.88	0.97
9e	1	4-CH_3O-C_6H_4	246	-5.09	-7.13	2.03	0.97
9g	1	2-Naphtyl	376	-4.83	-6.91	2.08	0.96
10d	2	4-CH_3-C_6H_4	554	-4.59	-6.75	2.16	1.03
10e	2	4-CH_3O-C_6H_4	749	-4.41	-6.59	2.18	0.99
11d	3	4-CH_3-C_6H_4	175	-5.29	-7.41	2.12	0.95
11e	3	4-CH_3O-C_6H_4	283	-5.00	-6.98	1.98	0.98
colchicine			0.058	-10.21	-11.80	1.59	1.01

Figure 5. Representative ITC binding isotherms for **6c** (A), **6f** (B), **7e** (C), **9c** (D), **9f** (E), and **10e** (F) titrations into tubulin solutions. Panel A, insert: example of ITC raw data.

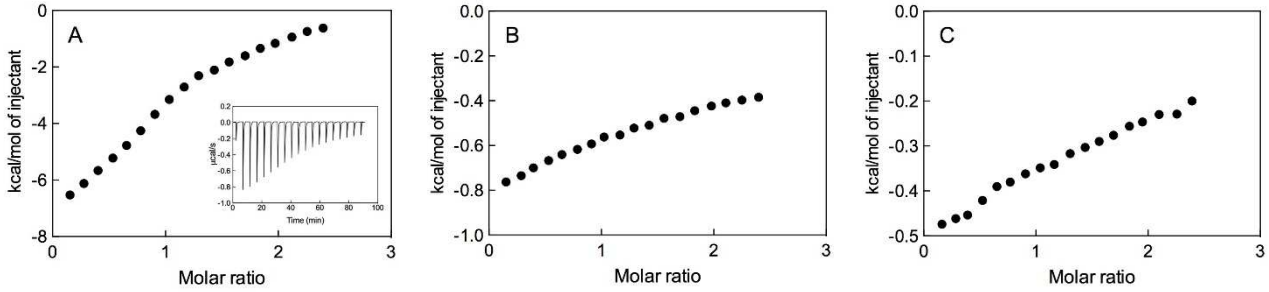

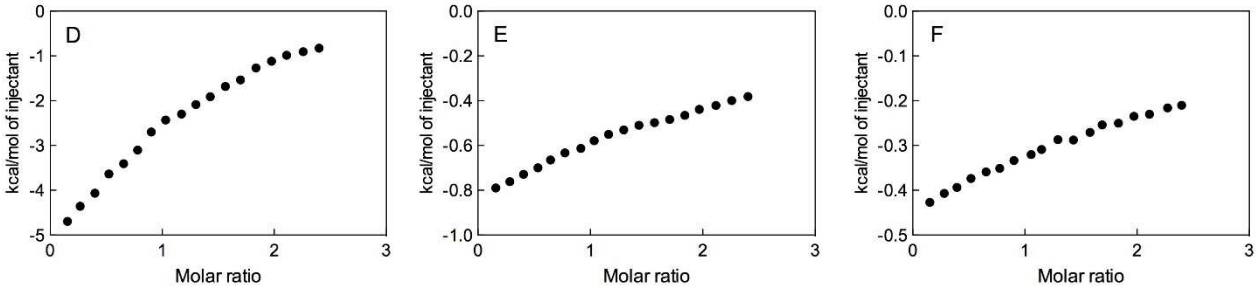

For the two series of compounds, the interaction with tubulin resulted in an exothermic ligand-binding event, with K_d values in the range 16.4 - 763 μM and 33.6 - 749 μM for the (**6-8**) and (**9-11**) compounds, respectively. Importantly, the ITC-derived K_d value for compound **6c** (16.4 μM) is nicely in agreement with the value obtained from the corresponding tubulin fluorescence quenching experiment (19.6 ± 1.0 μM). Generally speaking, the tubulin-compound binding is driven by the simultaneous participation of stabilizing van der Waals and hydrophobic interactions ($\Delta H_b < 0$), while entropy slightly disfavor complex formation ($T\Delta S_b > 0$). The conformational entropy change is commonly unfavorable in protein-ligand binding event, as the binding process involves the loss of configurational degrees of freedom for both the drug molecule and the protein, resulting in an ultimate negative change in conformational entropy. However, the presence of the planar bicyclic scaffold characterizing all present compounds confers a degree of overall molecular rigidity, which reflects only in a confined, unfavorable entropic contribution to ligand binding.

The last row in Table 2 shows the binding thermodynamic parameters for colchicine, used as a reference compound. The corresponding K_d value of 58 nM, in line with previous findings, confirm that all title compounds were consistently weaker than colchicine in their interaction with tubulin.

To understand whether the cytotoxic effect of the present (**6-8**) and (**9-11**) derivatives is dependent on their antimicrotubule activity, we next examined the relationship between the K_d values determined by the ITC tubulin binding assay and EC_{50} values in the cell-based assays. Since cytotoxicity tests were performed on 9 different human tumor cell lines, for the purpose of this comparison a single $EC_{50,av}$ value, corresponding to half-maximal inhibitory concentration value averaged over all cell lines, was employed. As shown in Figure 6, the resulting average EC_{50} vs. K_d plot show a highly positive correlation ($R^2 = 0.980$), suggesting a strong correlation between (**6-8**) and (**9-11**) compounds tubulin binding and cytotoxic potency. Therefore, we could conclude that the cytotoxic activity of both (**6-8**) and (**9-11**) derivatives is largely attributed to their antimicrotubule action.

Figure 6. Correlation between tubilin binding activity (K_d) and average cytotoxic activity ($EC_{50,av}$) of compounds **(6-8)** (●) and **(9-11)** (▲).

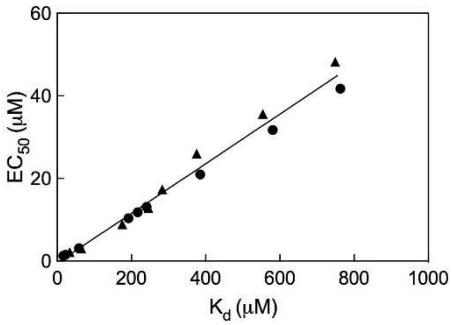

Microtubule-destabilizing compounds often bind tubulin by nesting into specific binding sites. In a previous work [8] we assessed the capability of a series of related compounds to compete with colchicine or paclitaxel for binding to tubulin by resorting to a competitive scintillation proximity assay. According to that study [8], we found that those compounds competitively inhibited [^{3}H]colchicine binding to biotinylated tubulin while they did not compete with [^{3}H]paclitaxel. In this work, however, we resorted again to ITC to examine whether the present compounds do compete either with colchicine or paclitaxel for the respective binding sites. With respect to the competitive scintillation proximity assay, the ITC-based experiments offers several advantages, including a clear determination of eventual binding site competition and, above all, to avoid working with radioligands.

Accordingly, we investigated the binding of compound **6c** to purified tubulin in the presence of colchicine or paclitaxel using ITC. Panel A of Figure 7 shows the typical exothermic profiles obtained for tubulin titration by **6c** at 37°C either in the presence of colchicine (thick black data) or in the presence of paclitaxel (light gray data). Figure 7 B shows the corresponding binding isotherms, i.e. the integrated heats of reaction as a function of the **6c**/tubulin molar ratio, in these two conditions.

Figure 7. A: ITC raw data obtained by titrating **6c** into a solution containing tubulin in the presence of colchicine (thick black curve) or paclitaxel (light gray curve). B: corresponding integrated heats of reaction in the presence of colchicine (■) or in the presence of paclitaxel (●).

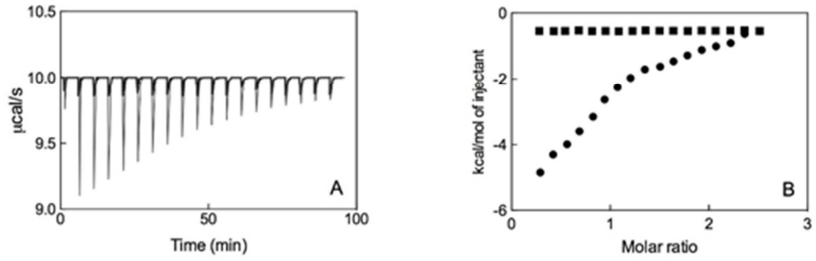

As can be easily seen from Figure 7B, in the presence of colchicine the tubulin binding of **6c** is completely abrogated. Colchicine is a very tight tubulin binder, with K_d = 58 nM (Table 2). Accordingly, **6c** (K_d = 16.4 μM) it is not able to displace colchicine from its tubulin binding site, as expected. Moreover, the fact that the titration of the tubulin-colchicine complex with **6c** returned a completely flat curve is a clear indication that, upon saturation of all tubulin binding sites by colchicine, **6c** is no longer able to interact with the protein, i.e., **6c** binds tubulin at the colchicine binding site. On the contrary, the binding isotherm resulting from the titration of tubulin by **6c** in the presence of paclitaxel (Figure 6B, circles) is practically coincident with that obtained in its absence (Figure 4A). Accordingly, **6c** does not interact with tubulin by binding at the paclitaxel binding pocket.

7. Molecular modeling rationale for the binding of compounds (6-8) and (9-11) to tubulin

In order to determine the structural basis of the biological results discussed above, the binding ability of the synthesized compounds to the colchicine binding site of α,β-tubulin was investigated using a consolidated molecular modeling procedure based on the combination of docking and Molecular Mechanics/Poisson-Boltzmann Surface Area (MM/PBSA)-based scoring techniques. Specifically, for this analysis we considered a subset of 3 compounds for each series, namely **6c**, **6f**, **7e**, **9c**, **9f**, and **10e**, as representative of strong, moderate, and weak tubulin binders, respectively (Table 2 and Figure 5). Table 3 reports the results of this *in silico* analysis. As seen by comparing the entries in Tables 2 and 3, all ligands are correctly ranked for affinity, the magnitudes of the calculated $\Delta G_{b,calc}$ (and of the corresponding $K_{d,calc}$) values being in excellent agreement with those determined experimentally.

Table 3. *In silico* binding thermodynamics of a subset of compounds (**6-8**) and (**9-11**) on human tubulin. The calculated value for colchicine is also reported for comparison.

Cpd	Pos. "N"	R	$K_{d,calc}$ (μM)	$\Delta G_{b,calc}$ (kcal/mol)	$\Delta H_{b,calc}$ (kcal/mol)	$T\Delta S_{b,calc}$ (kcal/mol)
6c	1	4-Br-C_6H_4	17.8	-6.70 ± 0.27	-23.07± 0.15	16.37 ± 0.23
6f	1	2-Naphtyl	371	-4.84 ± 0.24	-18.88 ± 0.11	14.04 ± 0.21
7e	2	4-CH_3O-C_6H_4	635	-4.51 ± 0.23	-18.09 ± 0.13	13.58 ± 0.19

Cpd	Pos. "N"	R	$K_{d,calc}$ (μM)	$\Delta G_{b,calc}$ (kcal/mol)	$\Delta H_{b,calc}$ (kcal/mol)	$T\Delta S_{b,calc}$ (kcal/mol)
9c	1	4-Br-C_6H_4	37.3	-6.24 ± 0.19	-22.16 ± 0.12	15.92± 0.15
9f	1	2-Naphtyl	436	-4.74 ± 0.26	-18.57 ± 0.13	13.83 ± 0.23
10e	2	4-CH_3O-C_6H_4	798	-4.37 ± 0.25	-17.23 ± 0.11	12.86 ± 0.22
colchicine			0.067	-10.12± 0.22	-24.11± 0.12	13.99 ± 0.18

It is interesting to observe that, with respect to the experimental values (Table 2), both $\Delta H_{b,calc}$ and $-T\Delta S_{b,calc}$ are substantially overestimated by the MM/PBSA calculations (Table 3); yet, since a parallel shift is observed between experimental and computed ΔH and –TΔS, (see Figure S1) their difference (i.e., $\Delta G_{b,calc}$) is ultimately close to the relevant experimental value (ΔG_b).

Concerning the binding mode of these new acrylonitrile derivatives, it has to be noticed that all compounds are provided with the chemical functions required for mapping the 3D pharmacophore model previously developed for tubulin inhibitors with a similar scaffold [8]. Indeed, taking the new lead compound **6c** as a meaningful example, all pharmacophore elements could be easily fitted by the proper molecular features, as shown in Figure 8A. Specifically, the triazolopyridinyl ring matches both the hydrophobic aromatic (HYAr) and the first hydrogen bond acceptor (HBA) features, while the cyano nitrogen atom overlays the second HBA. Finally, the 4-Br-C_6H_4enyl substituent maps the ring aromatic (RA) feature, presenting the aromatic ring in the proper conformation to optimize this molecular requirement (Figure 8A).

Figure 8. A: Mapping of compound **6c** onto the 3D pharmacophore model developed for structurally-related tubulin inhibitors [8]. The 3D pharmacophoric hypothesis features are portrayed as meshed spheres, color-coded as follows: light green, HBA; light blue, HYAr; light orange, RA. Compound **6c** is shown as atom-colored sticks-and-balls (gray, C; blue, N; dark red, Br; white, H). B: Equilibrated MD snapshots of tubulin/**6c** complex. The image is a zoomed view of the binding site. The ligand is portrayed as in panel A, while the protein residues mainly involved in the interaction with **6c** are highlighted as colored sticks and labelled. H-bonds interactions are shown as dotted black lines. Hydrogen atoms, water molecules, and ions are omitted for clarity.

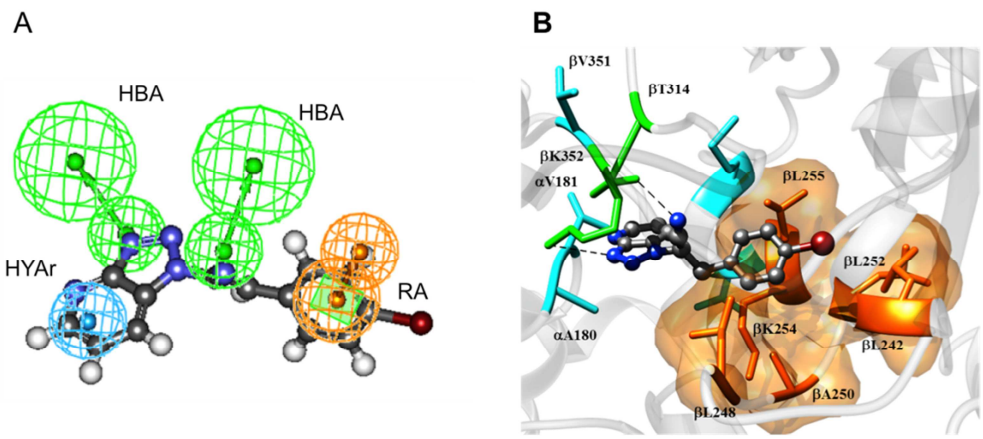

Our Molecular Dynamics (MD) simulations that allowed us to give a precise description of the binding mode of these new compounds have confirmed this interactions pattern. In fact, its combination with the relevant per-residue decomposition analysis of the binding enthalpy (ΔH_{res}) provided both the identification of the tubulin residues mainly involved in ligand binding and the nature underlying each specific interaction (Figure 8B and Figure 9A).

Figure 9. A: Comparison of the per-residue binding enthalpy decomposition (ΔH_{res}) for compounds **6c** and **7e** in complex with tubulin. Only those amino acids critical for the binding are shown. B: Superposition of equilibrated binding pose of **6c** (purple) and **7e** (red) in the tubulin binding cavity.

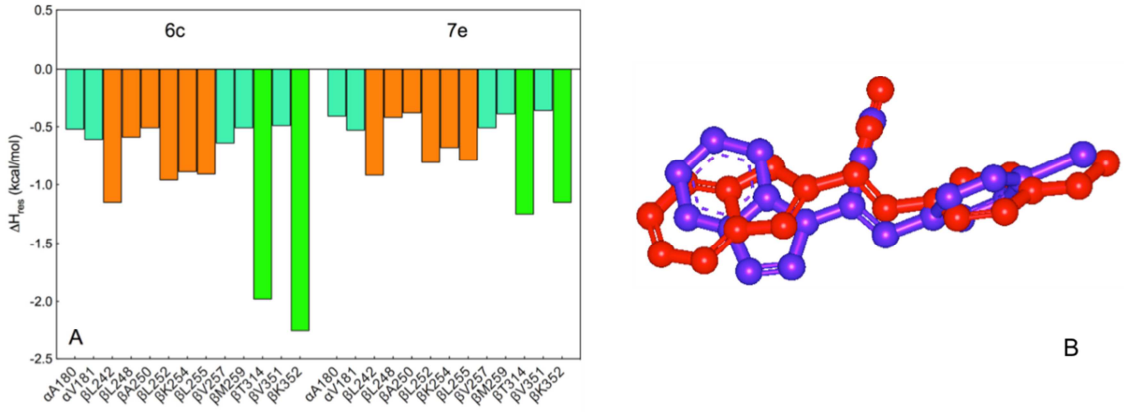

As can be seen in Figure 8B, the *p*-bromophenyl ring of **6c** is perfectly encased in the protein binding pocket lined by residues βL242, βL248, βA250, βl252, βK254 and βL255, and the deriving hydrophobic stabilizing interactions provided an overall contribution of -5.01 kcal/mol to the binding (Figure 9A). Furthermore, the donor guanidinium group of βK352 on the receptor finds its acceptor counterpart in the triazole N3 of the inhibitor, forming a persistent hydrogen bond (average dynamic distances (ADL) = 2.1 ± 0.1 Å) which yields a corresponding stabilizing contribution of ΔH_{res} = -2.26 kcal/mol. The triazolepyridinyl moiety is embedded in a hydrophobic pocket consisting of the side chains of αA180, αV181, βV257, βM259, and βV351 which all concur to foster a network of hydrophobic interactions with the ligands ($\sum\Delta H_{res}$ = -2.77 kcal/mol, Figure 9A). Finally, the cyano N atom is engaged in a permanent hydrogen bond with the hydroxyl group of the side chain of βT314 (ADL = 2.3 ± 0.2 Å; ΔH_{res} = -1.98 kcal/mol).

The same analysis applied to the other tested compounds, allowed us to confirm the structure-activity relationship proposed above (based on the *in vitro* results), and the related experimental data. First, all compounds demonstrated similar binding modes within the same tubulin binding pocket, the position of the substituted acrylonitrile moiety with respect to the triazolpyridinyl ring (N1, N2, or N3) modulating their protein binding affinity. Indeed, compounds featuring

substitutions at the N1 position are endowed with the highest tubulin affinity; yet, substitutions at position N3 is also well tolerated, the pyridine nitrogen atom not being involved in any specific interaction. On the other hand, compound **7e** (taken as a representative example of the N2 substituted derivatives) exhibits a substantially lower affinity compared to e.g., **6c**, as the conformation it assumes in the tubulin binding site (Figure 9B) does not satisfy all molecular determinants requested by the pharmacophore model. Specifically, the orientation of the chemical groups of **7e** involved in hydrogen bonds with tubulin residues βT314 and βK352 leads to a weaker interactions both in terms of dynamics stability (ADL = 2.8 ± 0.1 Å and ADL = 2.7 ± 0.3 Å for βT314 and βK352, respectively) and enthalpic contribution (ΔHβT315 = -1.55 kcal/mol and ΔHβK252 = -1.77 kcal/mol, Figure 9A). This, in turn, locally reflects into a sub-optimal encasement of **7e** in both protein hydrophobic pockets (thereby resulting into a lower stabilization energy of the protein residues directly involved in such specific interactions (Figure 9A), and globally into a less favorable $\Delta G_{b,calc}$ value for this molecule (Table 3).

8. Conclusions

In this work we presented the synthesis and *in vitro* anticancer activity of a new series of *E* isomers of triazolo[4,5-*b*/*c*]pyridin-acrylonitrile derivatives (**6c-g**, **7d-e**, **8d-e**, **9c-f**, **10d-e**, **11d-e**). All compounds were found to exert moderate to interesting antiproliferative activities against 9 different cancel cell lines derived from solid and hematological human tumors. Fluorescence-based assays proved that these molecules interfere with tubulin polymerization, and isothermal titration calorimetry led to full tubulin/compound binding thermodynamics determination (i.e., K_d, ΔG_b, ΔH_b, and $T\Delta S_\beta$ values). Coupling all experimental information with *in silico* modelling of the interactions between tubulin and the title compounds allowed to conclude that the position of the pyridine nitrogen atom does not exert a significant influence on their binding affinity toward their target protein. On the contrary, the position of the different R substituents on the three N atoms of the triazole ring is the major molecular determinant for the biological activity of these molecules, the N1 and N3 position leading to more potent compounds with respect to those presenting the same Rs at the N2 position.

9. Experimental section

9.1. Synthetic methods

Melting points were determined by a Kofler hot stage or Digital Electrothermal apparatus, and are uncorrected. ^{1}H and ^{13}C-NMR spectra were recorded on a Varian XL-200 and on a Bruker Avance III 400 NanoBay instruments, using TGC-MS as internal standard. The chemical shift values are

reported in ppm (δ) and coupling constants (*J*) in Hertz (*Hz*). Signal multiplicities are represented by: s (singlet), d (doublet) and m (multiplet). GC/MS spectra were performed on combined HP 5790 GC/MS and on a triple quadrupole (API 2000, Applied Biosystem MDS SCIEX) apparatuses. Column chromatography was performed using 230-400 mesh silica gel (Merck silica gel 60). Light petroleum refers to the fraction with b.p. 40-60 °C. The analytical results for C, H, N and chlorine were within 0.4% of the theoretical values.

9.1.1. Starting materials, intermediates and known compounds

3*H*-[1,2,3]triazolo[4,5-*b*]pyridine (**1a**), 3,4-diaminopyridine, aldehydes, 2-chloroacetonitrile, triethylamine, acetic acid, organic solvents and inorganic reagents were commercially available. 3*H*-[1,2,3]triazolo[4,5-*c*]pyridine (**1b**) was prepared following a consolidated procedure [10].

9.1.1.1. 3*H*-[1,2,3]triazolo[4,5-*c*]pyridine (1b). Yield: 83%. M.p.: 81 °C. ^{1}H-NMR (DMSO-d_6): δ 9.47(s, 1H, CH-4); 8.47(d, 1H, CH-7, *J* = 8 *Hz*); 7.88 (d,1H, CH-6, *J* = 4.2 *Hz*). ^{13}C-NMR ($CDCl_3$): δ 143.21 (C), 141.72 (CH), 138.56 (CH), 128.34 (C), 111.45 (CH). GC/MS: 121 (M+H). Anal. Calcd for ($C_5H_4N_4$): C, 50.00; H, 3.36; N, 46.65. Found: C, 49.92; H, 3.27; N, 46.72.

9.1.2. General procedure for the preparation of the intermediates 2a-b, 3a-b, 4a-b.

2 g (16.6 mmol) of the appropriate 3*H*-[1,2,3]triazolo[4,5-*b*/*c*]pyridine (**1a,b**) were dissolved in 20 ml of dimethylformamide (DMF). 1.95 g (19.4 mmol) 2.68 ml of triethylamine and 2 g (26.5 mmol) 1.69 ml of chloroacetonitrile were added to the resultant solution. The whole mixture was heated under reflux for 12 h. After cooling, the triethylamine hydrochloride formed was filtered, and the solution was evaporated to dryness. The residue, dissolved in ether, was washes with water. Through evaporation of the extract, a residue containing the three isomers **2-4a** or **2-4b** was obtained. Isomers were separated by flash chromatography, elution with light petroleum-ethyl acetate 80:20 afforded desired compounds.

9.1.2.1. 3*H*-[1,2,3]triazolo[4,5-*b*]pyridine-3-carbonitrile (2a). Yield: 24%. M.p.: 56.8-57 °C. ^{1}H-NMR (DMSO-d_6): δ 8.86 (d, 1H, CH-5. *J* = 4.0 *Hz*); 8.66 (d, 1H, CH-7. *J* = 8.8 *Hz*); 7.61 (m, 1H, CH-6); 6.14 (s, 2H, CH_2). ^{13}C-NMR ($CDCl_3$): δ 151.53 (CH); 144.76 (C); 136.18 (C); 129.18 (CH); 120.96 (CH); 114.73 (C); 34. 27 (CH_2). GC/MS: 146 (M+H). Anal. Calcd for ($C_6H_3N_5$): C, 49.66; H, 2.08; N, 48.26. Found: C, 49.56; H, 2.19; N, 48.23.

9.1.2.2. 2*H*-[1,2,3]triazolo[4,5-*b*]pyridine-2-carbonitrile (3a). Yield: 16%. M.p.: 98.6-100 °C. ^{1}H-NMR (DMSO-d_6): δ 8.89 (d, 1H, CH-5, *J* = 4.0 *Hz*); 8.53 (d, 1H, CH-7, *J* = 8.8 *Hz*); 7.61-7.55 (m,

1H, CH-6); 6.34 (s, 2H, CH_2). ^{13}C-NMR ($CDCl_3$): δ 155.15 (C); 153.21 (CH); 128.01 (C); 136.52 (C); 127.57 (CH); 123.41(CH); 114.06 (C); 44.57 (CH_2). GC/MS: 146 (M+H). Anal. Calcd for ($C_6H_3N_5$): C, 49.66; H, 2.08; N, 48.26. Found: C, 49.61; H, 2.10; N, 48.18.

9.1,2,3. 1*H*-[1,2,3]triazolo[4,5-*b*]pyridine-1-carbonitrile (4a). Yield: 38%. M.p.: 160-160.5 °C. ^{1}H-NMR (DMSO-d_6): δ 8.80 (d, 1H, CH-5, *J* = 4 *Hz*); 8.50 (d, 1H, CH-7, *J* = 8.4); 7.74-7.70 (m, 1H, CH-6); 6.22 (s, 2H, CH_2). ^{13}C-NMR ($CDCl_3$): δ 156.54 (C); 148.89 (CH); 125.16 (C); 123.30 (CH); 120.12 (CH); 114.79 (C); 36.38 (CH_2). GC/MS: 146 (M+H). Anal. Calcd for ($C_6H_3N_5$): C, 49.66; H, 2.08; N, 48.26. Found: C, 49.59; H, 2.15; N, 48.24.

9.1.2.4. 3*H*-[1,2,3]triazolo[4,5-*c*]pyridine-3-carbonitrile (2b). Yield: 19%. M.p.: 70-71 °C. ^{1}H-NMR (DMSO-d_6): δ 9.50 (s, 1H, CH-4); 8.59 (d, 1H, CH-7, *J* = 2.8 *Hz*); 8.17 (d, 1H, CH-6 *J* = 6*Hz*); 6.30 (s, 2H, CH_2). ^{13}C-NMR (DMSO): δ 148.26 (C); 142.51 (CH); 136.06 (CH); 129.57 (C); 114.70 (C); 112.90 (CH); 36.49 (CH_2). GC/MS: 146 (M + H). Anal. Calcd for ($C_6H_3N_5$): C, 49.66; H, 2.08; N, 48.26. Found: C, 49.61; H, 2.10; N, 48.29.

9.1.2.5. 2*H*-[1,2,3]triazolo[4,5-*c*]pyridine-2-carbonitrile (3b). Yield: 16%. M.p.: 99-100 °C. ^{1}H-NMR (DMSO-d_6): δ 9.58 (s, 1H, CH-4); 8.51 (d, 1H, CH-7, *J* = 6 *Hz*); 7.98 (d, 1H, CH-6, *J* = 6*Hz*); 6.41 (s, 2H, CH_2). ^{13}C-NMR (DMSO): δ 146.14 (C); 145.61 (CH); 143.21 (CH); 141.22 (C); 113.91 (C); 111.59 (CH); 44.55 (CH_2). GC/MS: 146 (M + H). Anal. Calcd for ($C_6H_3N_5$): C, 49.66; H, 2.08; N, 48.26. Found: C, 49.65; H, 2.03; N, 48.26.

9.1.2.6. 1*H*-[1,2,3]triazolo[4,5-*c*]pyridine-1-carbonitrile (4b). Yield: 28%. M.p.: 80-81 °C. ^{1}H-NMR (DMSO-d_6): δ 9.56 (s, 1H, CH-4); 8.68 (d, 1H, CH-7, *J* = 5.8 *Hz*); 8.01 (d, 1H, CH-6 *J* = 4.6*Hz*); 6.21(s, 2H, CH_2). ^{13}C-NMR (DMSO): δ 145.39 (CH); 144.16 (CH); 142.30 (C); 136.10 (C); 114.73 (C); 105.30 (CH); 33.51 (CH_2). GC/MS: 146 (M + H). Anal. Calcd for ($C_6H_3N_5$): C, 49.66; H, 2.08; N, 48.26. Found: C, 49.62; H, 2.04; N, 48.30.

9.1.3. General procedure for the preparation of [1,2,3]triazolo[4,5-*b/c*]pyridin-acrylonitrile derivatives.

To a solution of appropriate triazolo[4,5-*b*/*c*]pyridine-carbonitrile (**2a-b**, **3a-b**, **4a-b**) (1.4 mmol) and Et_3N (4.0 mmol) in toluene (5 mL) stirred at room temperature, a solution of a selected aldehyde **5c-g** (14 mmol) in the same solvent (3 mL) was added drop wise. The whole mixture was finally heated under reflux for 24 h. the solution was evaporated to obtain a crude residue containing a mixture of three E-isomers. The desired compounds were obtained by chromatography on silica gel column using light petroleum-ethyl acetate as eluent.

9.1.3.1. (*E*)-2-(1*H*-[1,2,3]triazolo[4,5-*b*]pyridin-1-yl)-3-(4-bromophenyl)acrylonitrile (6c). Yield: 53%. M.p.: 174-175 °C. ^{1}H-NMR ($CDCl_3$): δ 8.87 (d, 1H, CH-5, *J* = 4.4 *Hz*); 8.38 (d, 1H,

CH-7, *J* = 8.0 *Hz*), 8.04 (s, 1H, CH); 7.80 (d, 2H, CH 2′-6′, *J* = 3.8 *Hz*); 7.70 (d, 2H, CH-3′-5′, *J* = 3.8 *Hz*); 7.61 (m, 1H, CH-6). ^{13}C-NMR ($CDCl_3$): δ 157.85 (C); 149.31 (CH); 138.98 (CH); 132.83 (2 CH); 130.99 (2 CH); 129.09 (C); 127.02 (C); 124.21 (C); 123.65 (CH); 119.45 (CH); 113.16 (C), 106.68 (C). GC/MS: 326 (M+H). Anal. Calcd for ($C_{14}H_8BrN_5$): C, 51.56; H, 2.47; Br, 24.50. Found: C, 51.60; H, 2.51; Br, 24.47.

5.1.3.2. (*E*)-2-(1*H*-[1,2,3]triazolo[4,5-*b*]pyridin-1-yl)-3-(*p*-tolyl)acrylonitrile (6d). Yield: 53%. M.p. = 111-112 °C. ^{1}H-NMR (DMSO-d_6): δ 8.86 (d, 1H, CH-5. *J* = 4.4 *Hz*); 8.60 (d, 1H, CH-7. *J* = 8.0 *Hz*), 8.27 (s, 1H, CH=); 7.91 (d, 2H, CH-2',6', *J* = 7.8 *Hz*); 7.78 (m, 1H, CH-6); 7.45 (d, 2H, CH-3′,5′, *J* = 7.8 *Hz*); 2.49 (s, 3H, CH_3). ^{13}C-NMR ($CDCl_3$): δ 157.76 (C); 149.16 (CH); 144.82 (C); 143.48 (CH); 130.21 (2 CH); 129.86 (2 CH); 127.44 (C); 124.33 (C); 123.46 (CH); 119.45 (CH); 113.69 (C); 105.02 (C); 21.65 (CH_3). GC/MS: 262 (M+H). Anal. Calcd for ($C_{15}H_{11}N_5$): C, 68.95; H, 4.24; N, 26.80. Found: C, 68.99; H, 4.26; N, 26.78.

9.1.3.3. (*E*)-2-(1*H*-[1,2,3]triazolo[4,5-*b*]pyridin-1-yl)-3-(4-methoxyphenyl)acrylonitrile (6e). Yield: 35%. M.p. = 65.5-66 °C. ^{1}H-NMR (DMSO-d_6)*: δ* 8.86 (d, 1H, CH-5. *J* = 4.0 *Hz*); 8.58 (d, 1H, CH-7, *J* = 8.0 *Hz*), 8.23 (s, 1H, CH=); 7.80 (d, 2H, CH-2',6', *J* = 4.2 *Hz*); 7.76 (m, 1H, CH-6); 7.20 (d, 2H, CH-3′,5′, *J* = 4.2 *Hz*); 7.18 (m, 1H, CH, *J* =4.2 *Hz*); 3.88 (s, 3H, CH_3); ^{13}C-NMR ($CDCl_3$): δ 162.99 (C); 149.36 (CH); 141.29 (CH); 132.29 (2 CH); 131.71 (C); 124.40 (C); 123.25 (CH); 122.73 (C); 119.65 (CH); 115.27 (2 CH); 114.08 (C); 103.22 (C); 55.64 (CH_3). GC/MS: 278 (M+H). Anal. Calcd for ($C_{15}H_{11}N_5O$): C, 64.97; H, 4.00; N, 25.26. Found: C, 65.00; H, 4.03; N, 25.24.

9.1.3.4. (*E*)-2-(1*H*-[1,2,3]triazolo[4,5-*b*]pyridin-1-yl)-3-(naphthalen-2-yl)acrylonitrile (6f). Yield: 20%. M.p.: 186-187 °C. ^{1}H-NMR ($CDCl_3$): δ 8.87 (d, 1H, CH-5, *J* = 2.0 *Hz*); 8.41 (d, 1H, CH-7, *J* = 4.2 *Hz*); 8.34 (s, 1H, CH); 8.22 (s, 1H, CH-2′); 8.11 (d, 1H, CH-8′); 8.01-7.91 (m, 3H, napht); 7.66-7.60 (m, 3H, H-6 + 2H napht.). ^{13}C-NMR ($CDCl_3$): δ 157.85 (C); 149.24 (CH); 140.89 (CH); 134.88 (C); 132.90 (C); 132.17 (CH); 129.44 (CH); 128.99 (CH); 128.64 (CH); 128.23 (CH); 127.96 (CH); 127.67 (C); 127.39 (CH); 125.30 (C); 124.49 (CH); 123.54 (CH); 119.53 (CH); 113.69 (C); 105.93 (C). GC/MS: 298 (M+H). Anal. Calcd for ($C_{18}H_{11}N_5$): C, 72.72; H, 3.73; N, 23.56. Found: C, 72.69; H, 3.88; N, 23.61.

9.1.3.5. (*E*)-2-(1*H*-[1,2,3]triazolo[4,5-*b*]pyridin-1-yl)-3-(3,4,5-trimethoxyphenyl)acrylonitrile (6g). Yield: 35%. M.p.: 158-159 °C. ^{1}H-NMR ($CDCl_3$): δ 8.78 (d, 1H, CH-5. *J* = 8.4 *Hz*); 8.36 (d, 1H, CH-7, *J* = 8.4 *Hz*), 7.97 (s, 1H, CH); 7.61 (m, 1H, CH-6); 7.27 (s, 2H, CH-2′,5′); 3.97 (s, 3H, CH_3); 3.96 (s, 6H, 2 CH_3). ^{13}C-NMR ($CDCl_3$): δ 157.72 (C); 153.56 (2 C); 149.19 (CH); 141.88 (C); 141.22 (CH); 125.24 (C); 124.35 (C); 123.53 (CH); 119.44 (CH); 113.88 (C); 107.55 (2 CH);

104.83 (C); 61.15 (CH_3); 56.36 (2 CH_3). GC/MS: 338 (M+H). Anal. Calcd for ($C_{17}H_{15}N_5O_3$): C, 60.53; H, 4.48; N, 20.76. Found: C, 60.57; H, 4.51; N, 20.74.

9.1.3.6. (*E*)-2-(2*H*-[1,2,3]triazolo[4,5-*b*]pyridin-2-yl)-3-(*p*-tolyl)acrylonitrile (7d). Yield: 26 %. M.p.: 200-201 °C. ^{1}H-NMR ($CDCl_3$): δ 8.89 (d, 1H, CH-5, *J* = 2.6 *Hz*); 8.61 (s, 1H, CH); 8.31 (d, 1H, CH-7, *J* = 8.6 *Hz*); 7.91 (d, 2H, CH-2′,6′, *J* = 8.8 *Hz*); 7.44-7.43 (m, 1H, CH-6); 7.34 (d, 2H, CH-3′,5′, *J* = 8.8 *Hz*); 2.45 (s, 3H, CH_3). ^{13}C-NMR ($CDCl_3$): δ 155.61 (C); 153.84 (CH); 143.62 (2 C); 138.89 (CH); 137.53 (C); 130.36 (2 CH); 130.19 (2 CH); 127.32 (CH); 123.47 (CH); 112.82 (C); 111.15 (C); 21.80 (CH_3). GC/MS: 262 (M+H). Anal. Calcd for ($C_{15}H_{11}N_5$): C, 68.95; H, 4.24; N, 26.80. Found: C, 68.99; H, 4.20; N, 26.83.

9.1.3.7. (*E*)-2-(2*H*-[1,2,3]triazolo[4,5-*b*]pyridin-2-yl)-3-(4-methoxyphenyl)acrylonitrile (7e). Yield: 27 %. M.P.: 160-162 °C. ^{1}H-NMR (DMSO-d_6): δ 8.93 (d, 1H, CH-5, *J* = 2.6 *Hz*); 8.76 (s, 1H, CH=); 8.56 (d, 1H, CH-7, *J* = 8.6 *Hz*); 8.11 (d, 2H, CH-2′,6′, *J* = 8.8 *Hz*); 7.62 (m, 1H, CH-6); 7.22 (d, 2H, CH-3′,5′, *J* = 8.8 *Hz*); 3.88 (s, 3H, CH_3). ^{13}C-NMR ($CDCl_3$): δ 163.09 (C); 154.25 (CH); 142.95 (C); 138.57 (CH); 137.60 (C); 132.88 (2 CH); 127.23 (CH); 123.80 (CH); 123.31 (C); 115.31 (2 CH); 113.21 (C); 109.61 (C); 55.63 (CH_3). GC/MS: 278 (M+H). Anal. Calcd for ($C_{15}H_{11}N_5O$): C, 64.97; H, 4.00; N, 25.26. Found: C, 64.01; H, 4.03; N, 25.22.

9.1.3.8. (*E*)-2-(3*H*-[1,2,3]triazolo[4,5-*b*]pyridin-3-yl)-3-(*p*-tolyl)acrylonitrile (8d). Yield: 53%. M.p. = 95-96 °C. ^{1}H-NMR (DMSO-d_6): δ 8.96 (d, 1H, CH-5. *J* = 4.4 *Hz*); 8.81 (d, 1H, CH-7, *J* = 8.6 *Hz*), 8.59 (s, 1H, CH); 7.94 (d, 2H, CH-2',6', *J* = 8.2 *Hz*); 7.7 (m, 1H, CH-6, *J* = 4.4 *Hz*, *J* = 8.6 *Hz*); 7.4 (d, 2H, CH-3',5', *J* = 8.2 *Hz*); 2.46 (s, 3H, CH_3). ^{13}C-NMR ($CDCl_3$): δ 151.03 (CH); 144.16 (C); 142.71 (C); 139.38 (CH); 137.66 (C); 130.13 (2 CH); 130.01 (2 CH); 129.84 (CH); 127.85 (C); 120.94 (CH); 113.45 (C); 105.76 (C); 21.72 (CH_3). GC-MS: 262 (M+H). Anal. Calcd for ($C_{15}H_{11}N_5$): C, 68.95; H, 4.24; N, 26.80. Found: C, 68.98; H, 4.21; N, 26.83.

9.1.3.9. (*E*)-2-(3*H*-[1,2,3]triazolo[4,5-*b*]pyridin-3-yl)-3-(4-methoxyphenyl)acrylonitrile (8e). Yield: 28%. M.p.: 144-145 °C. ^{1}H-NMR (DMSO-d_6): δ 8.91 (d, 1H, CH-5, *J* = 4.9 *Hz*); 8.76 (d, 1H, CH-7, *J* = 8.2 *Hz*), 8.45 (s, 1H, CH=); 7.99 (d, 2H, CH-2',6', *J* = 8.0 *Hz*); 7.68 (m, 1H, CH-6); 7.19 (d, 2H, CH-3',5', *J* = 8.0 *Hz*); 3.88 (s, 3H, CH_3). ^{13}C-NMR ($CHCl_3$): δ 162.70 (C); 151.93 (CH); 145.18 (C); 139.67 (CH); 137.57 (C); 131.92 (2 CH); 129.37 (CH); 123.12 (C); 120.84 (CH); 114.64 (2 CH); 113.87 (C); 103.95 (C); 55.56 (CH_3). GC/MS: 278 (M+H). Anal. Calcd for ($C_{15}H_{11}N_5O$): C, 64.97; H, 4.00; N, 25.26. Found: C, 64.99; H, 3.97; N, 25.19.

9.1.3.10. (*E*)-2-(1*H*-[1,2,3]triazolo[4,5-*c*]pyridin-1-yl)-3-(4-bromophenyl)acrylonitrile (9c). Yield: 36%. M.p. = 169-170 °C. ^{1}H-NMR ($CDCl_3$): δ 9.56 (s,1H, CH-4); 8.74 (d, 1H, CH-6, *J* = 5.6 *Hz*); 7.99 (s, 1H, CH); 7.88 (d, 1H, CH-7, *J* = 5.6 *Hz*); 7.80 (d, 2H, CH-3′,5′, *J* = 8.4 *Hz*); 7.70 (d, 2H, CH-2′,6′, *J* = 8.4 *Hz*). ^{13}C-NMR ($CDCl_3$): δ 146.77 (CH); 145.34 (CH); 143.44 (C); 139.34

(CH); 135.16 (C); 132.85 (2xCH); 131 (2xCH); 128.97 (C); 127.14 (C); 114.17 (C); 106.36 (C); 105.03 (CH). GC/MS: 326 (M+H). Anal. Calcd for ($C_{14}H_8BrN_5$): C, 51.56; H, 2.47; Br, 24.50; N, 21.47. Found: C, 51.60; H, 2.51; Br, 24.52; N, 21.43.

9.1.3.11. (*E*)-2-(1*H*-[1,2,3]triazolo[4,5-*c*]pyridin-1-yl)-3-(*p*-tolyl)acrylonitrile (9d). Yield: 51%. M.p. = 180-181 °C. ^{1}H-NMR (DMSO-d_6): δ 9.64 (s, 1H, CH-4); 8.74 (d, 1H, CH-6, *J* = 5.4 *Hz*), 8.27 (s, 1H, CH); 8.1 (d, 1H, CH-7, *J* = 5.8 *Hz*); 7.92 (d, 2H, CH=, *J* = 7.8 *Hz*); 7.45 (d, 2H, CH=, *J* = 7.8 *Hz*); 2.42 (s, 3H, CH_3). ^{13}C-NMR ($CDCl_3$): δ 146.86 (CH); 145.32 (CH); 143.52 (C); 143.36 (C); 141.58 (CH); 135.19 (C); 130.23 (2 CH); 129.95 (2 CH); 127.33 (C); 114.08 (C); 105.05 (CH); 104.63 (C); 21.80 (CH_3). GC/MS: 262 (M+H). Anal. Calcd for ($C_{15}H_{11}N_5$): C, 68.95; H, 4.24; N, 26.80. Found: C, 69.98; H, 4.21; N, 26.76.

9.1.3.12. (*E*)-2-(1*H*-[1,2,3]triazolo[4,5-*c*]pyridin-1-yl)-3-(4-methoxyphenyl)acrylonitrile (9e). Yield: 94%. M.p.: 195-196.7°C. ^{1}H-NMR (DMSO-d_6): δ 9.63 (s, 1H, CH-4); 8.73 (d, 1H, CH-6, *J* = 6.2 *Hz*), 8.22 (s, 1H, CH); 8.07 (d, 1H, CH-7, *J* = 6.2 *Hz*); 8.02 (d, 2H, CH=, *J* = 8.8 *Hz*); 7.21 (d, 2H, CH=, *J* = 8.8 *Hz*); 3.88 (s, 3H, CH_3). ^{13}C-NMR ($CDCl_3$): δ 163.07 (C); 146.39 (CH); 145.26 (CH); 145.20 (CH); 144.01 (C); 141.62 (CH); 135.37 (C); 132.04 (2 CH); 122.61 (C); 114.99 (2 CH); 113.89 (C); 105.01(CH); 102.81 (C); 55.29 (CH_3). GC/MS: 278 (M+H). Anal. Calcd for ($C_{15}H_{11}N_5O$): C, 64.97; H, 4.00; N, 25.26. Found: C, 64.99; H, 3.97; N, 25.21.

9.1.3.13. (*E*)-2-(1*H*-[1,2,3]triazolo[4,5-*c*]pyridin-1-yl)-3-(naphthalen-2-yl)acrylonitrile (9f). Yield: 43 %. M.p. = 188-189 °C. ^{1}H-NMR ($CDCl_3$): δ 9.57 (s, 1H, CH-4); 8.74 (d, 1H, CH-6, *J* = 6.0 *Hz*); 8.33 (s, 1H, CH); 8.15 (s, 1H, CH); 8.10 (d, 1H, CH-7, *J* = 6.0 *Hz*); 8.01-7.57 (m, 6H, CH). ^{13}C- NMR ($CDCl_3$): δ 146.62 (CH); 145.29 (CH); 143.42 (C); 141.22 (CH); 135.28 (C); 134.90 (C); 132.96 (C); 132.21 (CH); 129.46 (CH); 128.07 (CH); 128.79 (CH); 127.96 (CH); 127.48 (CH); 124.45 (CH); 114.14 (C); 113.49 (C); 105.81 (C); 105.13 (CH). GC/MS: 298 (M+H). Anal. Calcd for ($C_{18}H_{11}N_5$): C, 72.72; H, 3.73; N, 23.56. Found: C, 72.68; H, 3.80; N, 23.54.

9.1.3.14. (*E*)-2-(2*H*-[1,2,3]triazolo[4,5-*c*]pyridin-2-yl)-3-(p-tolyl)acrylonitrile (10d). Yield: 46.9%. M.p. = 194-195°C. ^{1}H-NMR (DMSO-d_6): δ 9.65 (s, 1H, CH-4); 8.84 (s, 1H, CH,), 8.56 (d, 1H, CH-6. *J* = 5.4 *Hz*); 8.03 (d, 1H, CH-7, *J* = 5.4 *Hz*); 8.00(d, 2H, CH-2′,6′, *J* = 8.8 *Hz*); 7.45 (d, 2H, CH-3′,5′, *J* = 8.8 *Hz*); 2.42 (s, 3H, CH_3). ^{13}C-NMR ($CDCl_3$): δ 146.74 (C); 145.57 (CH); 144.00 (C); 143.84 (CH); 141.76 (C); 139.70 (CH); 130.46 (2 CH); 129.95 (2 CH); 127.02 (C); 112.81 (C); 11.84 (CH); 110.94 (C); 21.84 (CH_3). GC/MS: 262 (M+H). Anal. Calcd for ($C_{15}H_{11}N_5$): C, 68.95; H, 4.24; N, 26.80. Found: C, 68.93; H, 4.27; N, 26.79.

9.1.3.15. (*E*)-2-(2*H*-[1,2,3]triazolo[4,5-*c*]pyridin-2-yl)-3-(4-methoxyphenyl)acrylonitrile (10e). Yield: 56%. M.p.: 171-172 °C. ^{1}H-NMR (DMSO-d_6): δ 9.65 (s, 1H, CH-4); 8.83 (s, 1H, CH,), 8.55 (d, 1H, CH-6. *J* = 6 *Hz*); 8.12 (d, 2H, CH-2′,6′, *J* = 8.6 *Hz*); 8.04 (d, 1H, CH-7, *J* = 6.2 *Hz*); 7.22 (d,

2H, CH-3′,5′, *J*=8.6 *Hz*); 3.89 (s, 3H, CH_3). ^{13}C-NMR (DMSO-d_6): *δ* 163.34 (C); 146.71 (C); 145.42 (CH); 143.75 (CH); 141.73 (C); 139.32 (CH); 132.68 (2 CH); 122.34 (C); 115.05 (2 CH); 113.21 (C); 111.47 (CH); 109.38 (C); 55.66 (CH_3). GC-MS: 278 (M+H). Anal. Calcd for ($C_{15}H_{11}N_5O$): C, 64.97; H, 4.00; N, 25.26. Found: C, 65.00; H, 4.02; N, 25.29.

9.1.3.16. (*E*)-2-(3*H*-[1,2,3]triazolo[4,5-*c*]pyridin-3-yl)-3-(p-tolyl)acrylonitrile (11d). Yield: 16%. M.p. = 152–153 °C. ^{1}H.NMR ($CDCl_3$): δ 9.50 (s, 1H, CH-4); 8.68 (d, 1H, CH-6, *J* = 5.6 *Hz*); 8.06 (d, 1H, CH-7, *J* = 5.6 *Hz*); 7.96 (s, 1H, CH); 7.86 (s, 2H, CH-2′,6′, *J* = 8 *Hz*); 7.37 (d, 2H, CH-3′,5′, *J* = 8 *Hz*); 2.47 (s, 3H, CH_3). ^{13}C-NMR ($CDCl_3$): δ 149.98 (C); 143.87 (C); 142.73 (CH); 141.91 (CH); 134.82 (CH); 130.2 (2 CH); 130.0 (2 CH); 129.15 (C); 128.80 (C); 114.51 (CH); 113.65 (C); 104.79 (C); 21.82 (CH_3). GC/MS: 262 (M+H). Anal. Calcd for ($C_{15}H_{11}N_5$): C, 68.95; H, 4.24; N, 26.80. Found: C, 69.00; H, 4.26; N, 26.78.

9.1.3.17. (*E*)-2-(1*H*-[1,2,3]triazolo[4,5-*c*]pyridin-1-yl)-3-(4-methoxyphenyl)acrylonitrile (11e). Yield: 30%. M.p. = 161-162 °C. ^{1}H-NMR (DMSO-d_6): δ 9.56 (s, 1H, CH-4); 8.66 (d, 1H, CH-6, *J* = 5.8 *Hz*), 8.33 (s, 1H, CH); 8.25 (d, 1H, CH-7, *J* = 5.8 *Hz*); 8.04 (d, 2H, CH-2′,6′, *J* = 9 *Hz*); 7.21 (d, 2H, CH-3′,5′, *J* = 9 *Hz*); 3.88 (s, 3H, CH_3). ^{13}C-NMR (DMSO-d_6): δ 162.42 (C); 148.66 (C); 143.06 (CH); 141.74 (CH); 136.35 (CH); 135.43 (C); 132.41 (2 CH); 128.74 (C); 122.71 (C); 114.87 (2 CH); 114.54 (C); 113.53 (CH); 105.98 (C); 55.62 (CH_3). GC/MS = 278 (M+H). Anal. Calcd for ($C_{15}H_{11}N_5O$): C, 64.97; H, 4.00; N, 25.26. Found: C, 65.01; H, 4.03; N, 25.30.

9.2. Cytotoxicity assay

All cancer cell lines were obtained from the German Collection of Microbiology and Cell Culture (DSMZ, Braunschweig, FRG).

Human peripheral mononuclerar blood cells (P10588), human pulmonary fibroblasts (P10551), and human prostate epithelial cells (P10953) were purchased from Innoprot (Derio, Spain).

Exponentially growing cells derived from human hematological tumors - CCRF-CEM (ACC-240, T-cell leukemia) and HL-60 (acute myeloid leukemia) - were seeded at an initial density of 1 x 10^5 cells/mL in 96 well plates in RPMI-1640 medium supplemented with 10% fetal calf serum (FCS), 100 units/mL penicillin G and 100 □g/mL streptomycin. Human cell lines derived from solid tumors - HeLa (ACC-57, cervix carcinoma), DU145 (ACC-261, prostate carcinoma), MCF-7 (ACC-115, breast adenocarcinoma), A-427 (ACC-234, small cell lung carcinoma), LCLC 103H (ACC-384, large cell lung carcinoma), DAN-G (ACC-249, pancreas carcinoma), and 5637 (ACC-35, urinary bladder carcinoma) - were also seeded at 1x10^5 cells/mL in 96 well plates in specific media supplemented with 10% FCS and antibiotics as above. Cell cultures were then incubated at 37°C in a humidified, 5% CO_2 atmosphere in the absence or presence of serial dilutions of test

compounds. Cell viability was determined after 96 h at 37°C by the 3-(4,5-dimethylthiazol-2-yl)-2,5-diphenyl-tetrazolium bromide (MTT) method.

Each test was prepared in triplicate, and the experiments were carried out three times. EC_{50} values were obtained by nonlinear regression (GraphPad Prism v. 6.0) and represent the concentration at which cell growth was inhibited by 50%.

9.3. In vitro tubulin polymerization assay

The purity of tubulin was estimated to be >97% using Coomassie Brilliant Blue stained SDS-PAGE. Tubulin was re-suspended in a buffer containing 25 mM PIPES, 1 mM EGTA, and 3 mM $MgCl_2$ with 1 M glutamate and was incubated without or with different concentrations of title compounds for 10 min on ice. After 10 min, 1 mM GTP was added to the reaction mixtures, and subsequently, the assembly kinetics of tubulin was monitored at 350 nm (37 °C) for 20 min using Spectramax M2e multi-mode microplate reader (Molecular Devices, CA, USA). Each test was run in triplicate. The steady-state tubulin assembly level in the absence of inhibitor was set to 100%. ITP IC_{50} values were obtained by sigmoidal fitting of steady state levels of tubulin assembly vs. drug concentration and represent the concentration for 50% inhibition of the maximum tubulin polymerization level. Three independent sets of experiments were performed.

9.4. Cell cycle analysis

To determine the effect of compounds **6c** and **6d** on the cell cycle, cells were seeded in 12-well plates at a density of 10^5 cells/mL and allowed to attach for 24 h. Cells were then incubated in the presence or absence (DMSO) of compounds **6c** and **6d** at a concentration of 2 □M for 24 h. DMSO was used for control. Next, cells were collected, washed and fixed in 70% ethanol in PBS at -20 °C. After leaving overnight, the fixed cells were pelleted and stained with Propidium Iodide (25 mg/ml)) in the presence of RNase A (40 mg/mL) containing 0.1% Triton X-100 for 30 min at 37 °C in dark. About 10,000 events were analyzed using a FACSCalibur flow cytometry system (BD BioSciences, San Jose, CA, USA). Distribution of cells in cell cycle was determined using the BD FACStation Software (v. 6.1).

9.5. Preliminary determination of the dissociation constant of compounds 6c to tubulin in vitro by fluorescence spectroscopy

Tubulin was incubated in the absence and presence of different concentrations of compound **6c** for 10 min at 37 °C. Tryptophan fluorescence of tubulin in the presence and absence of compound **6c** was monitored using an excitation wavelength of 295 nm in a 0.3 cm path length cuvette (FP-6500

spectrofluorometer JASCO, Tokyo, Japan). The dissociation constant K_d for the binding interaction of **6c** and tubulin was calculated by fitting the change in fluorescence data using GraphPad Prism software (v. 6.0). Three independent sets of experiments were performed.

9.6. Determination of the dissociation constant and tubulin binding site of compounds (6-8) and (9-11) by Isothermal Titration Calorimetry (ITC).

Isothermal titration calorimetry (ITC) experiments were performed with a MicroCal PEAQ-ITC calorimeter (Malvern, UK) at 37°C (cell volume = 280 μL). Thermodynamics of Tubulin/ligand complex formation was investigated in PEM buffered solutions with 0.1 mM GDP, as stabilizer agents. Specifically, a solution of tubulin (50μM, sample cell) was titrated with 19 step-by-step injections of 2μL volume of each compound (600 μM, syringe). Solutions and buffer were degassed for 30 min at room temperature under stirring at 750 rpm prior to each experiment. All experiments were run in triplicate. Data acquisition and analysis were performed using inbuilt Origin 7.0 to determine the binding stoichiometry (n) and thermodynamic parameters of the binding reaction.

9.7. Molecular modeling

All simulations were carried out using the *Pmemd* modules of Amber 16 [17], running on own CPU/GPU calculation cluster. Molecular graphics images were produced using the UCSF Chimera package (v.1.10) [18]. Chimera is developed by the Resource for Biocomputing, Visualization, and Informatics at the University of California, San Francisco (supported by NIGMS P41-GM103311). All other graphs were obtained using GraphPad Prism (v. 6.0).

9.7.1 Docking procedure

The optimized structures of title compounds were docked into the tubulin binding pockets using the optimized 3D structure of the tubulin taken from our previous work [8]. All docking experiments were performed with Autodock 4.2.6/Autodock Tools 1.4.6 [19] on a win64 platform. The resulting docked conformations were clustered and visualized; then, the structure of each resulting complex characterized by the lowest Autodock interaction energy in the prevailing cluster was selected for further modeling.

9.7.2. Molecular dynamics simulations

Each ligand/tubulin complexes obtained from the docking procedure was further refined in Amber 16 using the quenched molecular dynamics (QMD) method as previously described [see, for example, 8, 20-22 and reference therein]. Next, the best energy configuration of each complex

resulting from QMD was subsequently solvated by a cubic box of TIP3P water molecules [23] extending at least 10 Å in each direction from the solute. The system was neutralized and the solution ionic strength was adjusted to the physiological value of 0.15M by adding the proper amounts of Na^+ and Cl^- ions. Each solvated system was relaxed (500 steps of steepest descent followed by 500 other conjugate-gradient minimization steps) and then gradually heated to the target temperature of 37°C in intervals of 50 ps of constant volume-constant temperature (NVT) molecular dynamics (MD) simulations (Verlet integration method, time step = 1.0 fs). The Langevin thermostat was used to control temperature. During this phase of MD, the protein was restrained with a force constant of 2.0 kcal/(mol Å), and all simulations were carried out with periodic boundary conditions. Subsequently, the density of the system was equilibrated via MD runs in the isothermal-isobaric (NPT) ensemble, with a time step of 1 fs. All restraints on the protein atoms were then removed, and each system was further equilibrated using NPT MD runs at 37°C. Three equilibration steps were performed (4 ns each, time step = 2.0 fs). System stability was monitored by the fluctuations of the root-mean-square-deviation (rmsd) of the simulated position of the backbone atoms of tubulin with respect to those of the initial protein model. The equilibration phase was followed by a data production run consisting of 50 ns of MD simulations in the NVT ensemble. Data collection was performed on over the last 20 ns of each equilibrated MD trajectory were considered for statistical data collections. 1000 trajectory snapshots were analyzed for each compound/tubulin complex.

9.7.3. Free energy of binding analysis

The free energy of binding ΔG_b and its major components (ΔH_b and $T\Delta S_b$) between the selected compounds and tubulin was estimated by resorting to the well-validated Molecular Mechanics/Poisson-Boltzmann Surface Area (MM/PBSA) approach [24] implemented in Amber 16. The per residue binding free energy decomposition (interaction spectra) was carried out using the Molecular Mechanics/Generalized Boltzmann Surface Area (MM/GBSA) approach [25,26], and was based on the same snapshots used in the binding free energy calculation.

Acknowledgments

S.P. and E.L. gratefully acknowledge the Associazione Italiana per la Ricerca sul Cancro (AIRC) for the generous financial support (grant IG 2015 Id.17413 to S.P.).

References

[1] D.G.I. Kingston, Tubulin-Interactive Natural Products as Anticancer Agents, J. Nat. Prod., (2009) 507-515.

[2] S. Sengupta, S.A. Thomas, Drug target interaction of tubulin-binding drugs in cancer therapy**,** Expert Rev. Anticancer Ther., (2006) 1433-1447.

[3] M. Kavallaris, Microtubules and resistance to tubulin-binding agents, Nat. Rev. Cancer, 10 (2010) 194-204.

[4] J. Xi, X. Zhu, Y. Feng, N. Huang, G. Luo, Y. Mao, Development of a novel class of tubulin inhibitors with promising anticancer activities, Mol. Cancer Res., 11 (2013) 856-864.

[5] A. Mandhare, P. Banerjee, Therapeutic use of colchicine and its derivatives: a patent review, Expert Opin. Ther. Pat., 29 (2016) 1-18.

[6] A. Carta, P. Sanna, M. Palomba, L. Vargiu, M. La Colla, R. Loddo, Synthesis and antiproliferative activity of 3-aryl-2-(1H-benzotriazol-1-yl)acrylonitriles. Part III, Eur. J. Med. Chem. , 37 (2002) 891-900.

[7] A. Carta, M. Palomba, G. Boatto, B. Busonera, M. Mureddu, R. Loddo, Synthesis and antiproliferative activity of 3-aryl-2-[1H(2H)-benzotriazol-1(2)-yl]acrylonitriles variously substituted: Part 4, Farmaco, 59 (2004) 637-644.

[8] A. Carta, I. Briguglio, S. Piras, G. Boatto, P. La Colla, R. Loddo, M. Tolomeo, S. Grimaudo, A. Di Cristina, R.M. Pipitone, E. Laurini, M.S. Paneni, P. Posocco, M. Fermeglia, S. Pricl, 3-Aryl-2-[1H-benzotriazol-1-yl]acrylonitriles: a novel class of potent tubulin inhibitors, Eur. J. Med. Chem., 46 (2011) 4151-4167.

[9] A. Carta, P. Sanna, A. Bacchi, Synthesis of E/Z 3-(1H-Benzotriazol-1-yl)-3-(Pyridin-4-yl)acrylonitriles and E/Z 2-(3-Imino-2-Benzofuran-1(3H)-ylidene)acetonitiles. An unusual case of displacement of the benzotriazole ring, Heterocycles 57 (2002) 1079-1090.

[10] A. Carta, M. Loriga, S. Piras, G. Paglietti, M. Ferrone, M. Fermeglia, S. Pricl, P. La Colla, G. Collu, T. Sanna, R. Loddo, Synthesis and anti-picornaviridae in vitro activity of a new class of helicase inhibitors the N,N'-bis[4-(1H(2H)-benzotriazol-1(2)-yl)phenyl] alkyldicarboxamides, Med. Chem., 3 (2007) 520-532.

[11] P. Sanna, A. Carta, M.E. Rahbar Nikookar, Synthesis and antitubercular activity of 3-aryl substituted-2-(1H(2H)-benzotriazol-1(2)-yl) acrylonitriles, Eur. J. Med. Chem. , 35 (2000) 535-543.

[12] P. Sanna, A. Carta, L. Gherardini, M.E. Rahbar Nikookar, Synthesis and antimycobacterial activity of 3-aryl-3-cyclohexyl-and 3-heteroaryl-substistuted-2-(1H(2H)-benzotriazol-1(2)-yl)prop-2-enenitriles, prop-2-enamides and propenoic acids, Farmaco, 57 (2002) 79-87.

[13] H. Prinz, P. Schmidt, K.J. Böhm, S. Baasner, K. Müller, E. Unger, M. Gerlach, E.G. Günther, 10-(2-oxo-2-Phenylethylidene)-10H-anthracen-9-ones as highly active antimicrotubule agents: synthesis, antiproliferative activity, and inhibition of tubulin polymerization, J. Med. Chem., 52 (2009) 1284-1294.

[14] Y. Yamazaki, K. Tanaka, B. Nicholson,G. Deyanat-Yazdi, B. Potts, T. Yoshida, A. Oda, T. Kitagawa, S. Orikasa, Y. Kiso, H. Yasui, M. Akamatsu, T. Chinen, T. Usui, Y. Shinozaki, F. Yakushiji, B.R. Miller, S. Neuteboom, M. Palladino, K. Kanoh, G. Kenneth Lloyd,Y. Hayashi, Synthesis and structure-activity relationship study of antimicrotubule agents phenylahistin derivatives with a didehydropiperazine-2,5-dione structure, J. Med. Chem., 55 (2012) 1056-1071.

[15] W. Zhao, J.-K. Bai, H.-M. Li, T. Chen, Y.-J. Tang, Tubulin structure-based drug design for the development of novel 4β-sulfur-substituted podophyllum tubulin inhibitors with anti-tumor activity, Sci. Rep., 5 (2015) 10172 (DOI: 10.1038/srep10172).

[16] V. Chaudhary, J.B. Venghateri, H.P.S. Dhaked, A.S. Bhoyar, S.K. Guchhait, D. Panda, Novel combretastatin-2-aminoimidazole analogues as potent tubulin assembly inhibitors: exploration of unique pharmacophoric impact of bridging skeleton and aryl moiety, J. Med. Chem., 59 (2016) 3439-3451.

[17] D.A. Case, R.M. Betz, W. Botello-Smith, D.S. Cerutti, T.E.I. Cheatham, T.A. Darden, R.E. Duke, T.J. Giese, H. Gohlke, A.W. Goetz, N. Homeyer, S. Izadi, P. Janowski, J. Kaus, A. Kovalenko, T.S. Lee, S. LeGrand, P. Li, C. Lin, T. Luchko, R. Luo, B. Madej, D. Mermelstein, K.M. Merz, G. Monard, H. Nguyen, H.T. Nguyen, I. Omelyan, A. Onufriev, D.R. Roe, A. Roitberg, C. Sagui, C.L. Simmerling, J. Swails, R.C. Walker, J. Wang, R.M. Wolf, X. Wu, L. Xiao, D.M. York, P.A. Kollman, AMBER 2016, University of California, San Francisco (CA, USA), 2016.

[18] E.F. Pettersen, T.D. Goddard, C.C. Huang, G.S.Couch, D.M. Greenblatt, E.C. Meng, T.E. Ferrin, UCSF Chimera - a visualization system for exploratory research and analysis, J. Comput. Chem., 25 (2004) 1605-1612.

[19] G.M. Morris, R. Huey, W. Lindstrom, M.F. Sanner, R.K. Belew, D.S. Goodsell, A.J. Olson, AutoDock4 and AutoDockTools4: automated docking with selective receptor flexibility., J. Comput. Chem., 30 (2009) 2785-2791.

[20] A: Carta, I. Briguglio, S. Piras, P. Corona, R. Ibba, E. Laurini, M. Fermeglia, S. Pricl, N. Desideri, E.M.Atzori, P. La Colla, G. Collu, I. Delogu, R. Loddo, A combined in silico/in vitro approach unveils common molecular requirements for efficient BVDV RdRp binding of linear aromatic N-polycyclic systems, Eur. J. Med. Chem., 117 (2016) 321-334.

[21] F. Weber, S. Brune, F. Börgel, C. Lange, K. Korpis, P.J. Bednarski, E. Laurini, M. Fermeglia, S. Pricl, D. Schepmann, B. Wünsch, Rigidity versus flexibility: is this an issue in σ1 receptor ligand affinity and activity?, J. Med. Chem., 59 (2016) 5505-5519.

[22] I. Briguglio, R. Loddo, E. Laurini, M. Fermeglia, S. Piras, P. Corona, P. Giunchedi, E. Gavini, G. Sanna, G. Giliberti, C. Ibba, P. Farci, P. La Colla, S. Pricl, A. Carta, Synthesis, cytotoxicity and antiviral evaluation of new series of imidazo[4,5-g]quinoline and pyrido[2,3-g]quinoxalinone derivatives, Eur. J. Med. Chem., 105 (2015) 63-79.

[23] W.L. Jorgensen, J. Chandrasekhar, J.D. Madura, R.W. Impey, M.L. Klein, Comparison of simple potential functions for simulating liquid water., J. Chem. Phys., 79 (1983) 926-935.

[24] I. Massova, P.A. Kollman, Combined molecular mechanical and continuum solvent approach (MM-PBSA/GBSA) to predict ligand binding., Perspect. Drug Discov., 18 (2000) 113-135.

[25] V. Tsui, D.A. Case, Theory and applications of the generalized Born solvation model in macromolecular simulations, Biopolymers, 56 (2000) 275-291.

[26] A. Onufriev, D. Bashford, D.A. Case, Modification of the generalized born model suitable for macromolecules, J. Phys. Chem. B, 104 (2000) 3712-3720.

Highlights

We present a series of *E* isomers of triazolo[4,5-*b*/*c*]pyridin-acrylonitrile derivatives

All the derivates have been investigated for their antiproliferative activity

Fluorescence-based assays prove that derivatives interfere with tubulin polymerization.

Isothermal titration calorimetry provides full tubulin/compound binding thermodynamics.

In silico modelling of interactions between tubulin and the title compounds is reported